University of South Carolina

Scholar Commons

2017

Far-Field Optical Microscopy Based on Stimulated Emission Depletion

Yunxia Wang
University of South Carolina

Recommended Citation

FAR-FIELD OPTICAL MICROSCOPY BASED ON STIMULATED EMISSION
DEPLETION

By

Yunxia Wang

Bachelor of Electronic Information Engineering
Fujian Normal University, 2011

Master of Physical Electronics
Fujian Normal University, 2014

Submitted in Partial Fulfillment of the Requirements

For the Degree of Master of Science in

Biomedical Engineering

College of Engineering and Computing

University of South Carolina

2017

Accepted by:

Guiren Wang, Director of Thesis

Qian Wang, Reader

Cheryl L. Addy, Vice Provost and Dean of the Graduate School

DEDICATION

I dedicate my thesis to my family. A special feeling of gratitude to my loving parents, who always encourages me to study hard and overcome the difficulties I meet. To my sisters and brother, who have never left my side and encourage me to continue whenever I face tough situations.

ACKNOWLEDGEMENTS

Firstly, I wish to express my deepest gratitude to my research supervisors, Dr. Guiren Wang, for his academic supervision and guidance, constant support and encouragement, invaluable advice throughout my Master degree. Furthermore, I would like to thank Arkm Abdalrahman, David Westbury, Wei Zhao, Dr. Zhenhua Bai and all my colleagues in the lab for their help and support. Moreover, a special thanks to Dr. Qian Wang for his time, comments, and instructions as a member of my thesis committee. Finally, I would like to express my deep appreciation and love to my parents, my siblings, who are standing by me and encouraging me to move forward all the time.

ABSTRACT

Conventional lens-based (far-field) fluorescence microscopy is a widely used imaging technique with spatial resolution up to 150–350 nm. However, this technology cannot discern very small structural features, because the spatial resolution is limited by diffraction to about half of the wavelength of light ($\lambda/2$，λ is the wavelength of light). Hence, most of the developments in microscopy aim at improving resolution. In the past decades, stimulated emission depletion (STED) microscopy has been developed to bypass the diffraction limit for the application in biological imaging with resolution approaching the nanoscale. The basic principle of STED microscopy is to employ a doughnut-shape laser called the depletion laser which inhibits fluorescence emission and improves the resolution of the focal plane by depleting the peripheral fluorescence. Thereby, STED microscopy avoids the diffraction barrier and improves the spatial resolution. STED microscopy has been widely applied to address many problems in biology with both continuous wave and pulsed wave lasers.

Various fluorescent nanoparticles, therefore, are attractive for far-field super-resolution microscopy. During the past decades, fluorescent nanoparticles have been used as a fluorescent label, fluorescent probe or marker for super-resolution imaging in vitro andvivo. In our study, STED microscopy is one of the breakthrough technologies that belongs to far-field optical microscopy and can reach the nanoscale spatial resolution. We demonstrate a far-field optical microscopy based on pulsed-wave lasers with the violet (405 nm) and green lasers (532 nm) for excitation and STED, respectively. Firstly,

fluorescent dye - Coumarin 102 is applied to verify the stability and reliability of the STED microscopy. Then, one suitable nanoparticle is selected from three different kinds of nanoparticles (Silica Nanoparticles-NFv465, flouro-Max blue aqueous fluorescent nanoparticles, light yellow nanoparticles) based on their absorption and depletion spectrum and depletion efficiency under different depletion power. Light yellow fluorescent nanoparticles (LYs) are selected for characterizing the spatial resolution of the STED microscopy. Finally, the laser beams of the STED microscopy are utilized to scan along a glass slide, which is coated with the LYs. A two-dimensional image of the LYs pattern is established and compared with the confocal imaging, indicating that a spatial resolution (approximately 76.02 nm) has been obtained in the STED imaging so far. Even though the resolution of STED microscopy with pulsed-laser has the room to be improved, the present work shows that our lab has successfully built up the STED microscopy with the pulsed-laser.

TABLE OF CONTENTS

LIST OF FIGURES

x

CHAPTER 1

INTRODUCTION

1.1 FLORESCENCE MICROSCOPY

1.1.1 Basic concept of Fluorescence Microscopy

Fluorescence microscopy is one type of optical microscopies capable of obtaining detailed images of the sample by the high intensity laser beam exciting fluorophores in the sample. The fluorophore is one type of chemical substances which can emit different wavelength light by absorbing the light form the excitation laser (Lichtman and Conchello 2005). The emission of light from the fluorophores or other materials by absorbing light is a form of luminescence, called fluorescence. Fluorescence is a popularly utilized approach in biology. The fluorescence was firstly proposed by Dr. Stokes in 1852 to depict the mineral fluorspar that can emit the red light when it is radiated by the ultraviolet light source (Stokes 1853). The basic theory of the microscopes that utilizes the transmitted or reflected light was introduced by one group form Oxford University (Wilson and Sheppard 1984). However, the fluorescence microscopy that utilizes excited fluorescence differs from that of one which employs transmitted or reflected light. The primary distinction is that the transmitted or reflected light is coherent. Whereas, the fluorescence is a kind of incoherent light (Kimura and Munakata 1989). Fluorescence microscopy gradually has become the mainstream of microscopy applied into the biology due to its intrinsic selectivity

(Lichtman and Conchello 2005). Fluorescence microscopy provides the opportunity of observing cells in vivo and vitro, and allows researchers to investigate the cell mechanisms and cellular constituents, such as proteins, nucleic acids, and lipids, by using the fluorescence tagging (Hell 2007, Pankajakshan 2010).

Different fluorophores can be excited by different wavelengths of the lasers. The images of microscopy are produced by irradiating of the sample with laser beams and scanning the specific area, using the detector to collect the signal (Agard 1984). In recent years, a lot of the technical studies of microscopy have been done to enhance the performance, focusing on improving the contrast between the signal and the background (Dudovich, Oron et al. 2002). Typically, basic rules should be obeyed for obtaining the strongest fluorescence signal. For example, the fluorophores had better be excited at the peak wavelength of the excitation spectrum (λex). Meanwhile, the emission had better be chosen at the peak wavelength of the emission spectrum (λem) (Pankajakshan 2010).

Generally, every fluorophore has an obvious excitation and emission spectrum which can be distinguished easily from that of all the other fluorophores (Brazelton and Blau 2005). In the past several years, many researchers have focused on discovering new fluorophores as the fluorescent probes to label the objects of the study in the biological systems (Dean and Palmer 2014). In addition, researchers also developed various fluorescence microscopy, such as the 4-Pi confocal fluorescence microscopy, the near-field fluorescence microscopy, the far-field fluorescence microscopy, the confocal scanning fluorescence microscopy and two-photon, wide-field fluorescence microscopy, laser scanning fluorescence microscopy etc. (Kinosita, Ashikawa et al. 1988, Kimura and Munakata 1989, Denk, Strickler et al. 1990, Hell and Stelzer 1992, Hell and Stelzer 1992,

Klar and Hell 1999, Gustafsson, Shao et al. 2008). Until now, the fluorescence

microscopy has a higher resolution than its conventional counterpart (Cremer and Cremer

1974, Brakenhoff, Blom et al. 1979, Wilson and Sheppard 1984, Wright, Centonze et al.

1993). The fluorescence microscopy has realized the 2D and 3D imaging, studying the

imaging of nanoparticles, dyes, complicated cells, tissues and even embryos in 2D and

3D by gathering the emitted fluorescence at every plane. (Velliste and Murphy 2002,

Chen, Velliste et al. 2003, Shtengel, Galbraith et al. 2009, Vicidomini, Moneron et al.

2011).

1.1.2 Far-field fluorescence Microscopy

Meanwhile, the electron and scanning probe microscopy in which the use of light

was abandoned with the development of microscopy techniques (Binnig and Rohrer

1984). The near-field optical microscopy is induced by the scanning probe microscopy

(Lewis, Isaacson et al. 1984, Pohl, Denk et al. 1984), in which the sharp metal tip is

applied to restrict the inter-reaction of the specimen with light to a sub-diffraction spot

(Agard and Sedat 1983, Novotny, Sánchez et al. 1998, Shtengel, Galbraith et al. 2009).

Despite of their success, these microscopes still have not displaced the far-field light

microscopy as the most extensively used microscopy in the biological fields. Moreover, it

can scan sample and form the images in 2D or 3D at a rapid and high speed. More

importantly, the fluorescence plays a very important function, permitting to observe

numerous organelles and proteins in the different cells (Klar and Hell 1999). The

fluorescence microscopy has other technological merits, including the relatively deeper

penetration of specimen (Williams, Zipfel et al. 2001), the improvement of signal

intensity from effective detectors with a large-region which maybe is not sensitive to the

scattering emitted light, the suppressive photo-bleaching and background signal from the outer area of the focal plane and so on (Hell, Booth et al. 1998). Furthermore, the obvious superiority of far-field fluorescence microscopy is that almost every protein has the potential to be marked with a fluorescent probe and localize proteins precisely, and permits dynamic and minimally invasive imaging experiments of biological molecules of interest (Betzig, Patterson et al. 2006, Gustafsson, Shao et al. 2008, Kobayashi, Ogawa et al. 2009, Nagano 2009). Compared to far-field fluorescence microscopy, the electron and probe microscopies have many disadvantages, including the destruction of antigens, a lack of appropriate antibodies and non-specific binding of antibodies, and the lack of accessibility of antigens.(Watanabe, Punge et al. 2011). Unquestionably, the far-field fluorescence microscopy still is one of the most frequently noninvasive imaging tools in many fields like biological and medical science. This is because that, apart from more-sophisticated specimen handling, the electron, probe microscopies and near-field fluorescence microscopy are primarily limited to the imaging of surfaces (Klar and Hell 1999). The far-field fluorescence microscopy gradually becomes an extremely crucial tool to observe and study bio-molecules, pathways and events in the inside cell, tissues and even animals (Hell 2009, Vicidomini, Moneron et al. 2011). Finally, the far-field fluorescence microscopy characterizing resolution beyond the diffraction barrier would be extraordinary appealing. The knowledge builds the foundation for the advent of stimulated emission depletion (STED) microscopy.

1.2 STED MICROSCOPY

1.2.1 Diffraction Limit

Last four hundred years, it has taken the forefront in the biological researches,

ranging from the macro level to the micro and even certain cellular organelles level. However, the diffraction limit becomes a barrier of the resolution because of optics always having a wave nature. As a result, a vast amount of the super-resolution technologies to improve resolution have appeared in the recent decades. Until the middle of 1990s, the first feasible concept was proposed to break the diffraction limit (Hell and Wichmann 1994, Hell and Kroug 1995).

As we all known, Ernst Abbe was the first person to recognize the limited spatial resolution of optical microscopy at the end of the nineteenth century (Abbe 1873). Abbe's contributions to the diffraction greatly influence the development of microscopy in the last century. Abbe discovered that the objects could not be distinguished when they are close to approximate 1/3 of the wavelength of light. Because the smallest focal spot size that the diffraction permits is the 1/3 of wavelength of light, when the lights focus with a lens of high numerical aperture (Klar, Engel et al. 2001). As a result, the electron and probe microscopies using light have been abandoned because of Abbe's diffraction barrier (Dyba and Hell 2002). Based on its merits compared to other imaging methods, the far-field fluorescent microscopy has become a very popular imaging technique.

1.2.2 Advent of STED Microscopy Breaking Diffraction Limit

The arrival of confocal and multiphoton fluorescence microscopies indeed accelerated the development of 3-D imaging. These techniques, however, did not actually enhance the resolution yet (Sheppard and Kompfner 1978, Wilson and Sheppard 1984, Denk, Strickler et al. 1990). It is due to that the conventional far-field fluorescence microscopy cannot break the diffraction barrier, which is a widely used imaging technique with spatial resolution ranging from 150 to 350 nm (Abbe 1873).

In recent decades, several improvements of far-field optical microscopy have arisen to improve the resolution beyond the Abbe's diffraction limit (Gustafsson 2005, Bretschneider, Eggeling et al. 2007). Under this circumstances, the emergence of stimulated emission depletion (STED) microscopy is in response to the needs of microscopy development. STED microscopy, as one of the breakthrough technologies, still belongs to far-field optical microscopy and can defeat the diffraction limit, reaching the nanoscale spatial resolution. STED derives from the reversible saturated optical fluorescence transition concept (Klar, Engel et al. 2001, Dyba and Hell 2002, Westphal and Hell 2005, Hotta, Fron et al. 2010) and was first established by Hell and Wichmann (Hell and Wichmann 1994, Hell, Booth et al. 1998, Willig, Rizzoli et al. 2006) . The optical fluorescence transition demonstrates that the simulated emission can degrade the fluorescent state. However, conventional lens-based optical microscopy cannot discern very small structural features, because the spatial resolution is limited by diffraction to about half of the wavelength of light ($\lambda/2$，λ is the wavelength of light) (Huang and Zheludev 2009). Hence, most of the developments in microscopy aim at improving the resolution. In the past decades, STED microscopy (Hell and Wichmann 1994, Hell 2007) has been developed to bypass the diffraction limit for application in biological imaging with resolution approaching nanoscale. The basic principle of STED microscopy is to employ a second laser donut beam called the depletion laser to inhibit fluorescence emission and improve the resolution of the focal plane by depleting the peripheral fluorescence. The emergence of STED microscopy (Klar, Jakobs et al. 2000, Donnert, Keller et al. 2006, Willig, Rizzoli et al. 2006) indicated that the diffraction limit can be fundamentally broken. Thus, the fluorescence microscopy with the conventional optics

6

enables the resolution to achieve macro-molecular scale. STED microscopy avoids the

diffraction barrier and increases the spatial resolution. STED microscopy has been widely

applied to address many problems in biology with both continuous wave (Rankin, Kellner

et al. 2008, Westphal, Rizzoli et al. 2008) and pulsed lasers (Willig, Harke et al. 2007,

Wildanger, Rittweger et al. 2008).

In order to calculate the resolution of STED microscopy, the theoretical lateral

spatial resolution of STED microscopy is demonstrated in the equation (1) (Li, Liu et al.

2013).

$$\Delta x = \frac{\lambda}{2nsin\theta\sqrt{1+I/I_{sat}}} \tag{1}$$

In this equation, where λ, n, and θ are beam wavelength (Hell, Dyba et al. 2004,

Westphal and Hell 2005, Takasaki, Ding et al. 2013, Xie, Liu et al. 2013), refractive

index, and half aperture angle of the objective, respectively. I is the maximum of the

intensity of the doughnut, and Isat is the saturation intensity. Meanwhile, nsin(θ) stands

for the numerical aperture (NA) of the objective lens. The effective resolution of STED

microscopy is controlled by both NA and the square root of the saturation factor I/Isat.

1.3 THE STED MICROSCOPY WITH CW LASER AND PULSED LASER

The STED microscopy is restricted due to the expense of appropriate light sources

capable of switching the fluorescent ability of the dye off, availability, and wavelength

etc. (Rankin, Kellner et al. 2008). It is no doubt that the selecting of the light source for

STED microscopy plays a major role in simplifying and broadening the application of

STED (Westphal, Blanca et al. 2003, Wildanger, Rittweger et al. 2008). In addition,

Suitable light sources can benefit the resolution of STED microscopy, i.e. the shorter of

wavelength, the higher of resolution. Besides, the light sources that offer a spectrum of

STED wavelengths make it possible for the users to freely choose fluorophores for specimen tagging. Massive research has been done to search the new light sources for the STED microscopy. Until now, STED microscopy has been successfully displayed by employing the titanium sapphire (Klar, Jakobs et al. 2000, Donnert, Keller et al. 2006, Harke, Keller et al. 2008, Rankin, Moneron et al. 2011), diode (Westphal, Blanca et al. 2003), continuous wave (Willig, Harke et al. 2007), and supercontinuum laser sources (Auksorius, Boruah et al. 2008, Wildanger, Rittweger et al. 2008). For example, the STED microscopy with the pulsed-laser is firstly introduced by Stefan W. Hell and Jan Wichmann in the 1994 (Hell and Wichmann 1994). The STED microscopy with the continuous wave (CW) beams was proposed by Katrin I Willig etc. (Willig, Harke et al. 2007), which can highly simplify the setup of the STED microscopy. In the Brian R. Rankin's group, the STED microscopy with the multicolor stimulated Raman-scattering light source enables the simple implementation of multicolor imaging.It produces an output spectrum during multiple available wavelengths from green to red with potential for further extension (Rankin, Kellner et al. 2008).

According to the reports, the presented STED microscopy is mainly implemented by the pulsed lasers and CW lasers for excitation. Both of STED microscopies have inherent advantages and disadvantages respectively. Typically, the setup of the pulsed STED system is more complicated and expensive for the optical setup and additional electronic equipment: the pulse length has to be adapted to the requirements of the system, being aligned in time with complex electronics (Harke 2008). In contrast, CW lasers can simplify the setup procedures, which also lead to a price decrease of the system. Another important merit is that the CW microscopy can work with low peak

intensities. Because the photo-damage mechanisms scale with at least the square of the intensity of the irradiated light (Hopt and Neher 2001, Kuang, Zhao et al. 2010).

Generally, the expense of pulsed laser sources is much higher than those for the CW ones. For the pulsed ones, the availability of the excitation is narrower than the CW laser sources. For example, the most universal laser for the pulsed laser systems is Titanium: Sapphire laser, in which the wavelength is confined to the near-infrared region. Many different dyes can work in the visible wavelength region.it is expected that the laser can be shifted to the visible wavelength region. However, the shift requires a second extra laser system such as an optic parametric oscillator (OPO), leading to a quite complicated and expensive pulsed-STED setup in the visible range.

The obvious superiority of a pulsed system is that high intensities can be produced easily by a standard laser, which means that high intensities normally lead to high depletion efficiency. Ultimately, there will have a better resolution. Here we demonstrate that the application of pulsed light source in STED microscopy is more attractive for obtaining higher resolution than CW STED.

1.4 FLUORESCENT DYE USED IN STED MICROSCOPY

A broad range of available fluorescent dyes have been developed. The choice of the types of fluorescent dyes for STED is extremely crucial. Because the fluorescent dyes control the higher sub-diffraction resolution of STED microscopy. Based on the various reports, fluorescent dyes employed in the STED microscopy typically excite wavelength ranging from 440 nm to 637nm. More importantly, many fluorescent dyes have made an effect on the improvement of resolution for microscopy imaging technologies. Common fluorescent dyes include ATTO 633, ATTO 647N, ATTO 590, ATTO 594, ATTO435

and ATTO 932, etc. (Dyba, Keller et al. 2005, Kellner, Baier et al. 2007, Meyer, Wildanger et al. 2008, Punge, Rizzoli et al. 2008).

STED microscopy becomes a widely used instrument to investigate a variety of specimens by obtaining their noninvasive imaging. For the STED microscopy, the principle is that the stimulated emission has ability to deplete the fluorescent state, thereby making the focal areas of substance excitation smaller than the diffraction limit. For reaching a better sub-diffraction resolution, the selection of a fluorescent dye applied into STED microscopy is extremely vital. There mainly have two requirements for choosing a suitable dye. First, the dye had better be photo-stable with high fluorescence quantum yield under prolonged irradiation. Second, for making excitation process and the depletion process not affect each other, the absorbance and the fluorescence spectrum of the dye had better overlap as less as possible.

Over the past couple of decades, STED microscopy has a rapid development by a vast of studies with the target to improve the sub-diffraction resolution. Based on the reports, the previous study results show various fluorescent dyes with different excitation wavelength employed in microscopy. At red light band, ATTO 647N, ATTO 633 and JA 26 have been reported to have the smallest lateral resolution of 16 nm (Westphal, Blanca et al. 2003, Westphal, Kastrup et al. 2003, Westphal and Hell 2005, Westphal, Seeger et al. 2005, Punge, Rizzoli et al. 2008). At the orange light band, the fluorescent dyes of ATTO 590, Alexa 594 and ATTO 594 can have a minimum resolution reaching 20 nm in 2D plane (Meyer, Wildanger et al. 2008, Wildanger, Medda et al. 2009). At the yellow light band, Dyba et al reported that Pyridine 2 and RH 414 could reach the best resolution of 30 nm on z axis direction (Dyba and Hell 2002, Dyba, Keller et al. 2005). At the green

light band, more dyes had been validated in comparison with other light bands, containing ATTO565, MR 121 SE, NK51, etc. Rittweger et al employed Nitrogen vacancies in diamond to reach the smallest resolution of 6nm at the x-y plane (Dyba, Jakobs et al. 2003, Wildanger, Rittweger et al. 2008, Hell and Rittweger 2009). At the cyan light band, DY-485 XL, Alexa 488, etc. have been validated by a number of researchers, obtaining resolution up to 40 nm (Meyer, Wildanger et al. 2008, Moneron, Medda et al. 2010). At the blue light band, the resolution using ATTO 435 and ATTO 932 could achieve 25 nm (Donnert, Keller et al. 2006, Kellner, Baier et al. 2007, Meyer, Wildanger et al. 2008). At the violet light band, even though few fluorescent dyes have been studied, ATTO 390 still is validated to be suitable in STED microscopy. Briefly, various excitation wavelengths of fluorescent dyes have been investigated ranging from 440 nm to 637 nm. The requirement of choosing dyes should have photo-stability, have low overlap rate between the absorbance and the fluorescence spectrum, and own relatively long excited-state lifetimes. Furthermore, the different fluorescent dyes can obtain different best resolution in the microscopy imaging technologies. Therefore, selecting a suitable fluorescent dye becomes extraordinarily important for STED microscopy.

1.5 FLUORESCENT NANOMATERIALS APPLICATION IN STED MICROSCOPY

1.5.1 Aim of Fluorescent Nanomaterial Applied in STED Microscopy

In all kinds of stimuli-responsive signal types, fluorescent emission is outstanding and promising. There have two reasons. One is that fluorescent signal intensity can be easily and sensitively detected. Another reason is that fluorescence can be well monitored with many identifying characteristics, like wavelength, signal intensity, depletion efficiency, photo-bleaching and lifetime. Once the novel types of fluorescence

microscopy are employed, like STED microscopy, photo-switchable fluorescent nanomaterials significantly make an effect on improving the super-high resolution of the fluorescence imaging. Therefore, the different types of photo-switchable fluorescent nanomaterials are developed to play a key role in the biology and other fields. In addition, fluorescence nanomaterials expand the various researches and applications at the nano-meter level. The applicability of nanomaterials for the aims of imaging has created a variety of approaches for imaging with characteristics, consisting of the improvement of brightness, even the better distribution, and the inertness to micro-surrounding (Wolfbeis 2015).

Based on the theory of STED system, the bright fluorescence signal of samples passes through the objective and then the photo multiplier tube (PMT) or the avalanche photodiode (APD) is used to collect the signal. The fluorescent intensity could be depleted at any part except from the central part of the doughnut-shape spot. Unquestionably, the number of emitted photons of STED microscopy is significantly reduced in contrast with conventional confocal microscopy. As a result, the resolution of STED system is greatly improved. However, in term of the resolution equation, if we want to detect suitable signal and obtain high resolution, the choice of fluorophores exerts an important influence. Of course, the appropriate fluorophores for STED microscopy should follow to certain important requirements, consisting of high resistance to the photo-bleaching, short wavelength, high depletion rate, low overlap rate between the absorption and the emission spectrum, and relatively long excited-state lifetimes (Klar, Jakobs et al. 2000). In addition, the key character of suitable fluorophores is the value of *I/Isat*, which is larger, the resolution is higher, based on the equation (1).

Various fluorescent nanomaterials, therefore, are attractive for far-field super-resolution microscopy. Nano-materials not only can extend the application of STED system, but also can be applied as fluorescent probe to stain proteins, organelles etc. More importantly, they can provide help to address various and fundamental problems in the region of cell biology and medicine. Especially, the STED system can study the activities, biochemical and biophysical properties of cell nucleus, cytoplasm, organelles and membranes, even involving in probing and extracting the desired information at the spatial resolution of nanometer. Tremendous advances in STED techniques with high resolution allow single nanomaterial to label biomolecules, ions, and microstructures etc. in live cells, which is able to monitor the movement of nanomaterials in the real time. Meanwhile, the optical and biological properties of nanomaterials in live cells are also commendably summarized on the base of vast researches.

In the recent decades, a variety of nanomaterials have been studied by the STED system, consisting of carbon nanotubes (CNTs), quantum dots (QDs), metal clusters, up-conversional nanomaterials, fluorescent nano-diamonds, fluorescently doped silica and sol–gels, hydrophilic polymers (hydrogels), hydrophobic organic polymers, semiconducting polymer dots, and polystyrene (PS) nanoparticles etc. (Xu, Wang et al. 2007).

Take the quantum dots (QDs) as an example. Even though the QDs are frequently used in the optical bio-imaging, QDs are not very suitable for STED microscopy due to their broad absorption spectrum. For the STED beam, there has a big possibility for re-exciting an emitter, resulting in blurring of STED image and even seriously destroying the sample (Busko, Baluschev et al. 2012). Because of the deep exploration and research

in term of the QDs, a new discovery was published (Irvine, Staudt et al. 2008). The report showed that the absorption coefficient of Mn-doped ZnSe QDs could be negligible at λ >450 nm, but fluorescence is emitted at $\lambda max= 580$ nm. Obviously, the fluorescence could be effectively depleted by the stimulated emission at $\lambda= 664$ nm (Irvine, Staudt et al. 2008). A resolution could attain to 45 nm. Especially, the new appearance of various nanomaterials leads to the new and promising methods for diagnosis and therapy of certain diseases, including the therapy of cancers. The combination of therapeutic methods with diagnostic approaches such as imaging technology causese so-called theranostic nanomaterials. Carbon nanomaterials and carbon nanotubes are on the topmost of theranostic nanomaterials for the disease treatment. Moreover, the fluorescent nano-diamond (Tzeng, Faklaris et al. 2011) as a fluorescent label or marker can be used for in cells for super-resolution imaging. Therefore, the new discovery and exploration of florescent nanomaterials could have important significance for improving resolution in the fluorescence microscopy. However, on the other hand, the primary disadvantage of STED application is the lack of the ideality of existing nanomaterials with fluorophores. To find and explore more and more fluorescent nanomaterials become an important factor for achieving the theory with no limit of resolution for STED microscopy.

1.6 NANOPARTICLE APPLICATION IN THE STED MICROSCOPY

The common use of nanoparticles includes four aspects as following: plain fluorescence imaging of cells, targeted imaging, imaging of chemical species, and imaging of temperature (Tzeng, Faklaris et al. 2011). The nanoparticle without fluorescence is common such as hybrid nanoparticles (Klar, Jakobs et al. 2000) and gold nanoparticle. A considerable interest has been paid on hybrid nanoparticles owning to

14

their applicability in a number of significantly technological fields like energy conversion (Salerno and Daban 2003) and catalysis (Freeman, Finder et al. 2010). The largest challenge of using the STED microscopy is to get a perfect doughnut. The intensity of the perfect doughnut at the center should be less than 1% of the intensity of the maximum (Rittweger, Han et al. 2009). Furthermore, the overlap between STED and excitation beam, the uniform profile of doughnut and excitation has an important effect on attaining the best resolution. At this point, the gold nanoparticles play a vital role to check if the doughnut is optimal (Wildanger, Bückers et al. 2009).

Another popular nanoparticle is fluorescent nanoparticle applied in fluorescent imaging, mainly of cells and tissues in the STED microscopy. Fluorescent nanoparticles are extremely important due to their applicability in numerous significant fields such as biological and medical science (Santra, Dutta et al. 2005, Wildanger, Bückers et al. 2009). Additionally, the fluorescent nanoparticles as optical agents for applications in different types of cells are also becoming increasingly common. The fluorescent nanoparticles could be internalized by cells prior to the surgery, which is different from the fluorescent dyes and gadolinium chelates (Santra, Dutta et al. 2005, Wildanger, Bückers et al. 2009). Furthermore, the fluorescent nanoparticles can stay very well in the cell without the diffusion out of cells during the whole process of diagnose. Therefore, the fluorescent nanoparticle is a good and promising candidate for various researches in many technologically different fields at the nanoscale level.

Recently, a nanoparticle named CLIO-Cy5.5 has been developed, which can be applied into both an MRI contrast agent and a near-infrared fluorescent optical probe (Kircher, Mahmood et al. 2003). The fluorescent nano-diamonds are a new found of

fluorescent nanoparticles. Fluorescent nano-diamonds have great potential for use in biology and medicine (Vaijayanthimala and Chang 2009, Xing and Dai 2009). Especially, using the STED microscopy is current possible to collect diffraction-unlimited images of fluorescent nano-diamonds. The improvement of resolution by using the STED microscopy could observe the detailed structures of different and various samples, consisting of particularly small organelles and compartments. Based on super-resolution researches of fluorescent nano-diamonds, we can extend the study to the application of cellular-imaging.

From another point of view, nanoparticles have considerable advantages compared to the molecular probes, such as nontoxicity and unwanted sequestration. The bond of molecular probes by using cellular proteins could have an influence on the probes' optical properties and the proteins' function. In comparison, the fluorescent nanoparticles are substantially inactive, without interaction with cellular proteins and the influence of outer proteins on optical properties. More importantly, the photo-stability of fluorescent nanoparticles is more stable than those of molecular probes. Most nanoparticles could be readily internalized into both cells and tissues. Until now, many various kinds of nanoparticles are available on commercials.

Nanoparticles are regarded as an important tool applied into biology science. We can anticipate that the more types of nanoparticles are discovered as a type of photo-stable bio-labels and long-term cell trackers. The combination of the great photo-stability of fluorescent nanoparticles with STED microscopy is expected to produce many remarkable new opportunities to investigate intracellular mutual reaction and dynamic

changes with high super-high resolution and excellent precision (Tzeng, Faklaris et al. 2011).

1.7 THE PURPOSE OF THE STUDY

The microscopy should be one of the strongest instruments for researchers investigating in the various fields, especially in the biology. The microscopy makes it possible to study specimen and obtain the detailed information about the size, the appearance, the structure and even the optical properties of the investigated subjects. Therefore, it plays a key role in multifarious and interdisciplinary fields.

The microscopy technologies mostly are divided into two types: the near and the far-field optical microscopy. In general, the near-field microscopy has better resolution compared to the far-filed microscopy. The near-field microscopy like atomic force microscopy, scanning tunneling microscopy, and scanning optical microscopy has a better resolution than the far-field microscopy (Abbe 1873, Binnig and Rohrer 1987, Pohl and Courjon 2012). Whereas, all the approaches of the near-field microscopy mainly collect information from the surface of the samples, the information hidden below is hardly to be extracted. The conventional far-field microscopy, nonetheless, has the high penetration depth into the specimen. More importantly, the far-filed microscopy permits researchers to utilize the marker for meeting the required specificity. Therefore, more researchers focus on the development of far-field microscopy.

Obviously, the visualization of tiny and fine structures conduces greatly to a better explanation of the features of the study objects. Hence, the resolution is the most important characteristic of the microscopy, which demonstrates the capacity to recognize the position of compact objects. The resolution plays a decisive role for observing and

investigating the minute structure of the sample. Consequently, the mass of improvements in microscopy are emphasis on the better resolution. Obviously, the enhancement of resolution always results in the new discoveries and new breakthrough in different fields.

Furthermore, with the exception of bio-imaging, STED nanoscopy has also been successfully applied to nanoscopic measurement in micro- and nano-fluidics (Kazoe et al, 2011 ; Kuang et al, 2010). For instance, laser induced fluorescence photo-bleaching anemometer (LIFPA) is a new method that can measure flow velocity with simultaneously high spatial and temporal resolution (Zhao et al, 2016). With STED microscopy, LIFPA has the potential to measure the flow velocity profile in a nano-channel (Kuang et al, 2010) and interfacial flows, such as electrical double layers and slip flows. Developing new CDs that can be used for UV light could enable new applications of CDs to the measurement of flow velocity and concentration profiles in micro- and nano-fluidics in the future.

Therefore, we develop and align a kind of the pulsed-wave STED microscopy with excitation laser (405 nm) and the STED laser (532 nm). The aim of our experiment is to test the stability and reliability of the pulsed-wave STED system, and obtain the higher resolution in the STED image by comparing with the confocal image.

We first align the pulsed-laser STED microscopy by using the gold nanoparticle. Observe the focus points of both lasers through the camera and analyze the PFS of both lasers after scanning the gold nanoparticle. Then we use the coumarin 102 to test the stability and reliability of the STED system. And then we analyze the absorption and emission spectrum and measure the depletion efficiency of three kinds of nanoparticles for choosing one which is suitable for our STED system. Next, we utilize the pulsed-

18

wave STED microscopy to scan the sample of nanoparticles. To the end, we compare the confocal image with STED image, showing that the STED images have the higher resolution. Hence, this result illustrates that STED system is successfully aligned by our lab. In contrast to near-field scanning optical microscopy, this approach can produce three-dimensional images of translucent specimens.

CHAPTER 2

APPARATUS

2.1 BASIC STED MICROSCOPY APPARATUS

The setup of two-beam path STED microscopy is depicted in the Figure 2.1, which is featured with a wavelength of pulsed-wave 405 nm for excitation and a wavelength of pulsed-wave 532 nm for depletion, respectively. For excitation beam, the linear-polarized beam is guided through a lens–pinhole–lens system consisting of lens (L1), pinhole (PH1) and lens (L3) to enlarge the diameter of the beam. The beam is firstly reflected by a dichroic mirror (DM1) and then is reflected by a second dichroic mirror (DM2). For depletion beam, the linear-polarized beam is guided and enlarged by another lens-pinhole-lens system consisting of lens (L2), pinhole (PH2) and lens (L4). Then, the depletion beam passes through a l/2 wave plate and phase plate PP (Vortex phase plate VPP-1, RPC photonic Inc., NY). The wave plate enables the excitation beam to have the same direction with the depletion beam. Meanwhile, the phase plate can generate a doughnut pattern.

The excitation and depletion beams overlap and pass through a 1/4 wave plate WP2. The linear polarization beams are changed into circular pattern by the wave plate WP2, and reflected by a reflector R2 and then focused by an objective lens OL (100X, PlanApo, NA=1.4 oil immersions, Olympus, NY). The metallic reflector R2 can avoid messing up the circularity of the polarization. The sample is put between a cover slip and

a microscopy slide. In addition, it is fixed on a nano-cube NC piezo-scanning stage (P-611.3FS, PI Inc.), which can be scanned in all three spatial directions with a positioning resolution of 1 nm for fine tune. Rough tune is adjusted by three-axis manual translation stages. The fluorescent signal is collected by objective lens and goes through the two dichroic mirrors (DM1 and DM2). And then the signal is reflected by R1 and gathered by a photomultiplier tube (PMT). The preamplifier amplifies the signal, which is acquired by an A/D converter and saved to a computer.
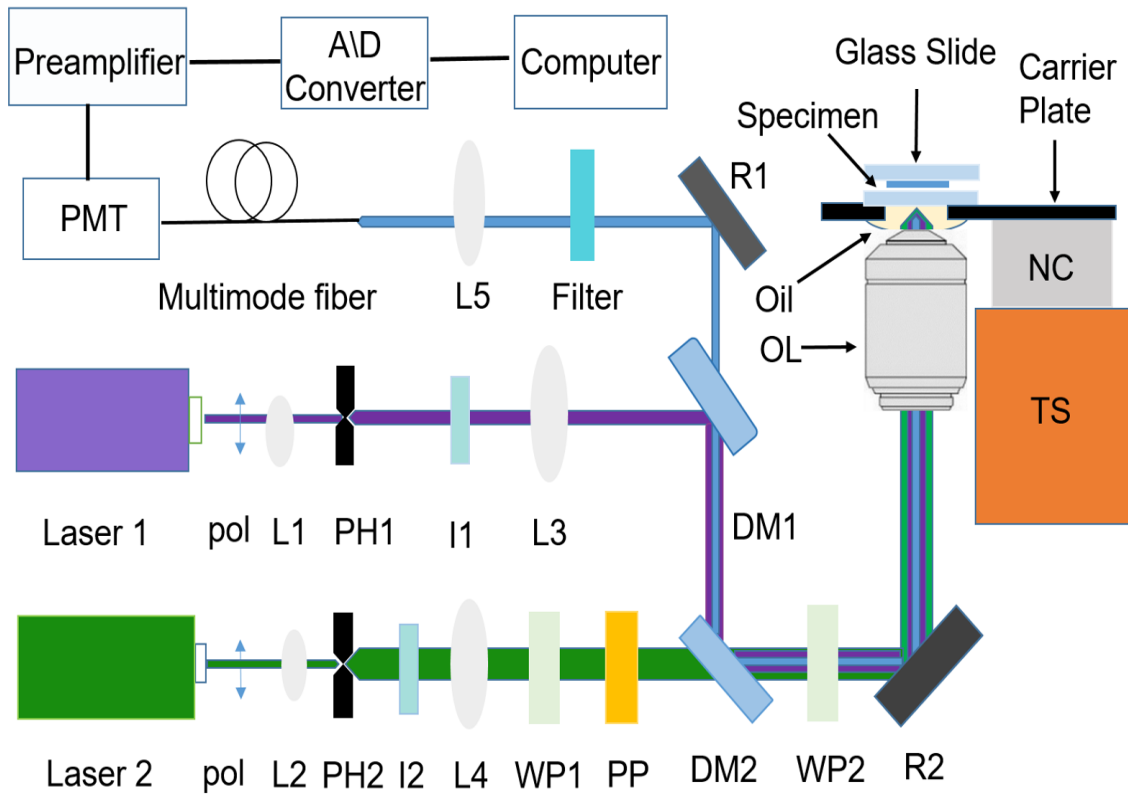
Figure 2.1 A schematic of the STED setup
Laser 1: continuous wave at 405 nm; laser 2: continuous wave at 532 nm; L1, L2, L3, L4 and L5: optical lenses; PH1 and PH 2: pinholes; I1 and I2: Iris; WP1 and WP2: wave plate (WP1: l/2, WP2: l/4); Pol: light polarization direction; DM1 and DM2: dichroic mirrors; PP: phase plate; PMT: photomultiplier tube; R1 and R2: reflector mirrors; OL: objective lens (PlanApo 100X, NA=1.4 oil immersion); NC: nano cube piezo scanner (3-axis); TS: translation stage, (3-axis)

2.2 ALIGNMENT OF STED MICROSCOPY

It has been known that the STED microscopy can arrive the super-resolution beyond the Abbe limit. The diffraction barrier is overcome by using the STED laser to quench the excited organic molecules at the edge of the focal area. Among the variety of super- resolution imaging techniques, STED microscopy is the most universal. STED microscopy utilizes the properties of fluorescence to produce a smaller effective point spread function (PSF). As a rule, the point spread function (PSF) always plays a very vital part in comprehending imaging effects and presentation, like the analytical resolution limit and the optical sectioning ability. For point-like illumination and detection, the distribution of PSF is dependent on the quality of the lens, the numerical aperture (NA) of the microscopy objective, and the wavelengths of the emission and excitation light (WA 1959). The PSF can distinguish the object points out of the focal region.

Hence, a crucial requisite for super-resolution STED is the quality of the effective doughnut-shaped point spread functions (PSFs). Before spontaneously fluorescing, the stimulated emission forces the excited fluorescent photons back to the ground state of STED microscopy. Besides, the fluorescence-depleting transition is regulated by another laser-depletion laser (Green Laser: 532nm). The focus point of the depletion laser characterizes a central intensity as zero which limits the sub-diffraction region from which fluorescent light is likely to be emitted and gathered. Herein, the STED microscopy demands accurate alignment, from the focus point of the center of the excitation laser to the focus point of intensity-zero depletion laser. In addition, STED laser can cause more photo-bleaching owing to switching on-off operation. Hence, it is

reasonable to adjust the power of the excitation to its smallest level of measurement for small particles or beads, especially when STED resolution requires to be measured.

The conventional way to align the focus point of the both laser is to image the scattered laser light from gold nanoparticle. However, Gold nanoparticles (<200nm) are generally employed, via detecting if the excitation PSF with the depletion doughnut PSF overlap very well in STED. Accordingly, the detection of PSF is normally much more difficult than imaging a specimen in the STED microscopy. Because the tip of the gold nanoparticle is hard to create the reflection signal. The method is very effective to measure the PSFs of both laser, modulating the position of the focus point for the aim of overlapping each other very well.

Yet, this traditional approach has some disadvantages. As mentioned above, the photo-bleaching is severe when first scan the gold nanoparticle with excitation laser and then scan the gold nanoparticle with depletion laser. Then, the specimen should be prepared with caution. This is because if the nanoparticles are distribution with high concentration, this is easy to generate self-accumulation, causing the problem which we could not detect the PSF accurately. Third, this approach mainly depends on manual operation to align the position of the focus of both lasers. Therefore, researchers put much attention on improving the STED alignment. Travis J etc. proposed to employ adaptive optics for achieving the purpose of automatically aligning STED microscopy [64]. Importantly, this approach can make spatial alignment of the focus point of excitation and depletion in the 3D imaging. One of crucial advantages is employing the feedback of the STED fluorescent images to guarantee the precise alignment, aiming at avoiding the imprecision caused by the mismatch of the fluorescent imaging modes and

23

reflection. In our lad, we previously used a different method to test whether the excitation and depletion lasers overlap very well. But the disadvantage of the method is not accurate enough.

The previous method: we manually used the reflection principle to adjust and modulate optical elements by multiple mirrors and a piece of white paper, visually checking the excitation and the STED beams whether they are aligned very well at the beginning. And then adjusted the manual PI stage (Physic Instrument P-611.3 Nano-Cube XYZ Piezo Stage), especially adjusted Z axis, to modulate a suitable position for obtaining the excitation and STED focus points. Then we used the cameras to observe the excitation laser focus point first, and then to observe the STED laser focus point. Finally, we observed the both laser focus points at the same time.

The scanning gold nanoparticle method: we tested the point-spread functions (PSFs) of the both focus points, verifying that the PSFs of both lasers were aligned very well in the focal plane. In the end, we measured the PSFs of both beams via scanning a gold nanoparticle with the excitation beam firstly, and then with the STED beam. The results are shown in the Figure 2.2, showing that both the excitation spot and STED spot overlap properly. However, we could see that the intensity of STED laser is not zero in the middle of STED focus spot. When we find that the excitation and STED beams cannot overlap very well, the STED system should be aligned again. Otherwise, you could not obtain high-resolution images, because the STED alignment plays a very important part in achieving high resolution for STED microscopy. What is more, the STED alignment is the foundation of the following experiments.

We first checked the focus points of excitation laser and depletion laser to see if
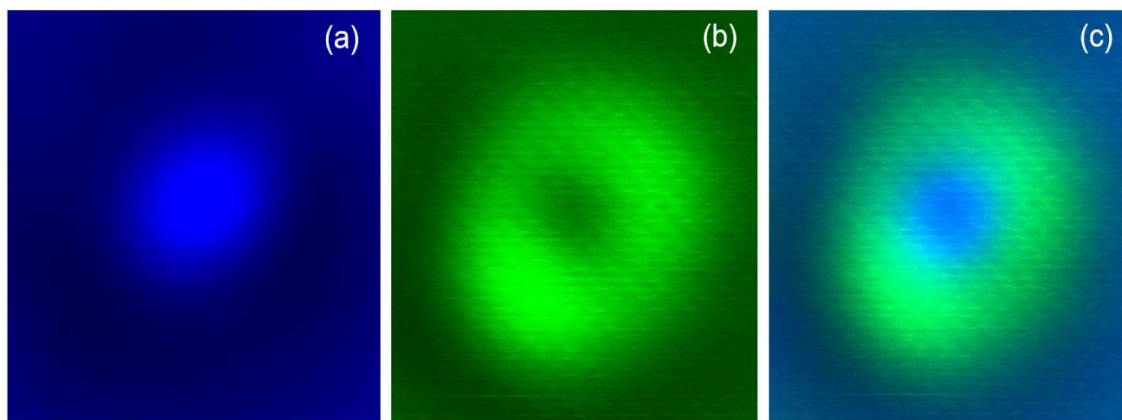
Figure 2.2 The overlap of the excitation and depletion focus points (a) Effective fluorescent spot (b) Excitation spot (c) STED spot.

they overlapped each other very well, showing in the Figure 2.2. Then we further got the intensity profile of the excitation and the STED beams by scanning the gold nanoparticle and analyzing them via the NIKON software, then checked whether they were properly aligned. The results of excitation and STED focus spots in the lateral (XY) and axial (XZ, YZ) directions, and intensity profiles in the lateral plane are clearly shown in Figure 2.3, verifying that the two PSFs of excitation and depletion lasers are aligned in the focal plane very well. The results shown in the Figure 2.3(a), (b) and (c) illustrate the STED focus spot and excitation focus spot overlap very well.

We could observe from Figure 2.3 (d), the excitation focus beam locates the middle of STED focus beam. We could notice that the intensity of STED laser is not very uniform in the figure 2.3 (a), (b) and (c). For more details, the result shown in the Figure (d) confirms that the intensity of STED laser is not inform and is not zero (about 1500) in the middle of focus spot. Meanwhile, we can easily see that the background noise is a little strong. On the other hand, the intensity profile of excitation laser is not very symmetrical, because the intensity of excitation laser could reach 2000 at the beginning, and the intensity of excitation laser almost achieves to 0 at the end. Even though these

disadvantages will affect the resolution of STED microscopy, this is the best focus spot

we could get currently. We will find new technologies and methods to improve these
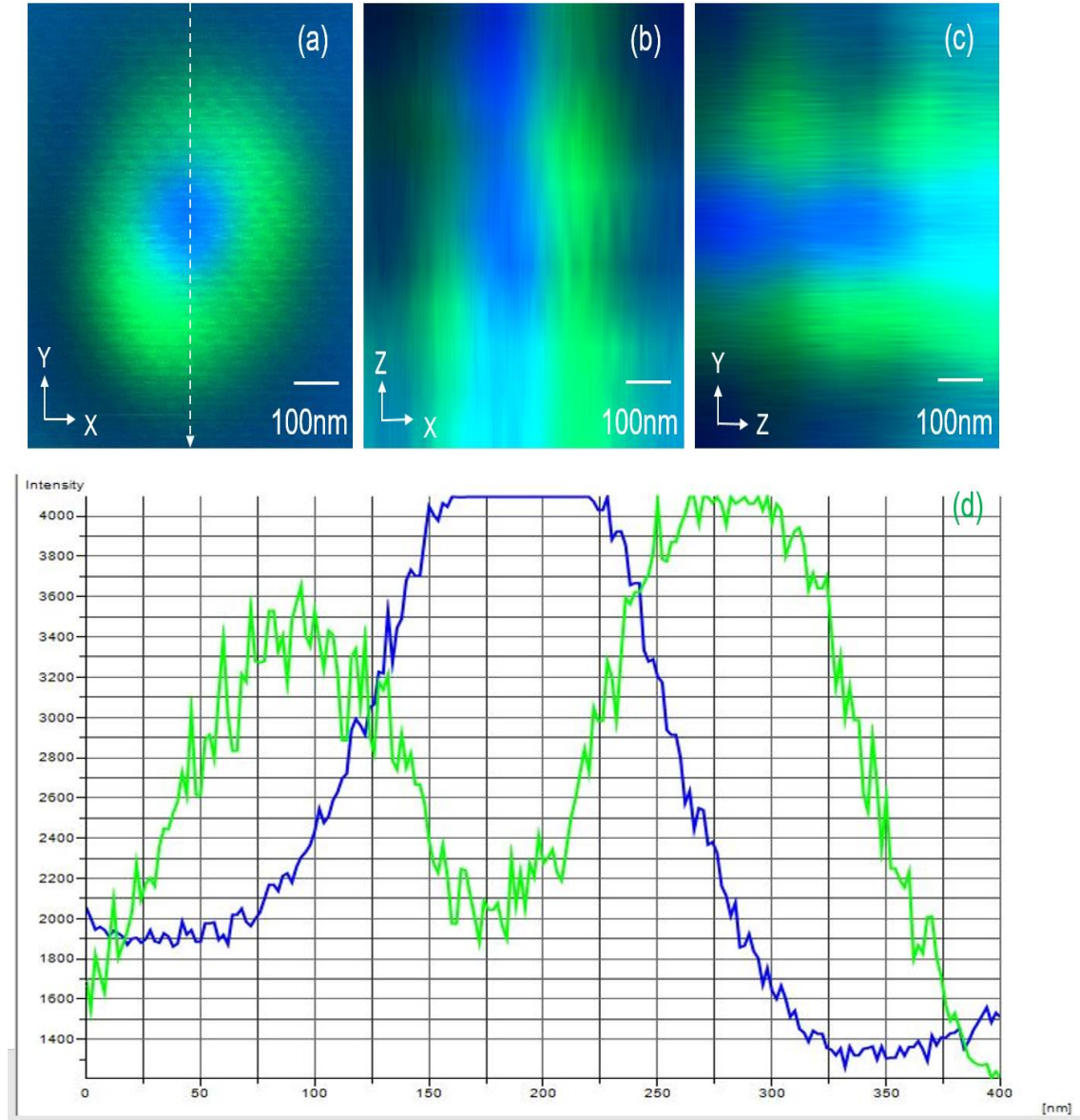
disadvantages in the future.

Figure 2.3 The focus point and intensity profile; (a) STED focus point at x-y plane (b)
STED focus point at x-z plane (c) STED focus point at y-z plane (d) Intensity profile
along the lines in the image (a).

.

2.3 TESTING THE POWER OF STED LASER

In our STED system, there have two the laser devices-green laser (532nm) and blue violet laser (405nm). But these two laser devices just have digital display without the corresponding laser power. In consequence, we first use the PowerMax-USB/RS sensors (Coherent.Inc.) to detect the power of the green laser, as shown in the Figure 2.4. Before doing this experiment, we firstly confirmed the model specifications of the PowerMax-USB/RS (mode number: 11742630), so that we could choose the right model to conduct this experiment. As shown in the table 2.1, the model 11742630 could accurately detect the power of STED laser.

In this experiment, we connected the PowerMax-USB/RS (Figure 2.4 (a)) to the computer, and opened the related software at this computer; then you can see the interface of the software (Figure 2.4 (b)). We used the PowerMax-USB/RS sensors to detect the green laser at the far end of STED system. Before putting the PowerMax-USB/RS sensor at the right position, we firstly clicked "zero sensor" on the interface of the software to make sure the initial power is zero when there is no any laser source. And then we put the PowerMax-USB/RS at the right position and changed the number of display screen of the green laser, then the corresponding power of green laser would show on the interface of PowerMax. Finally, recorded them carefully by using the Origin Software, and depicted the relevant curve line, showing the number on screen corresponding with power of green laser (Figure 2.5). In the Figure 2.5, w the power of the green laser device is in proportion to the number on screen. This experiment will help us to determine power of green laser, choose the suitable power of green laser for reducing the photobleaching, and improve the resolution.

Table 2.1 The parameter of PowerMax USB.

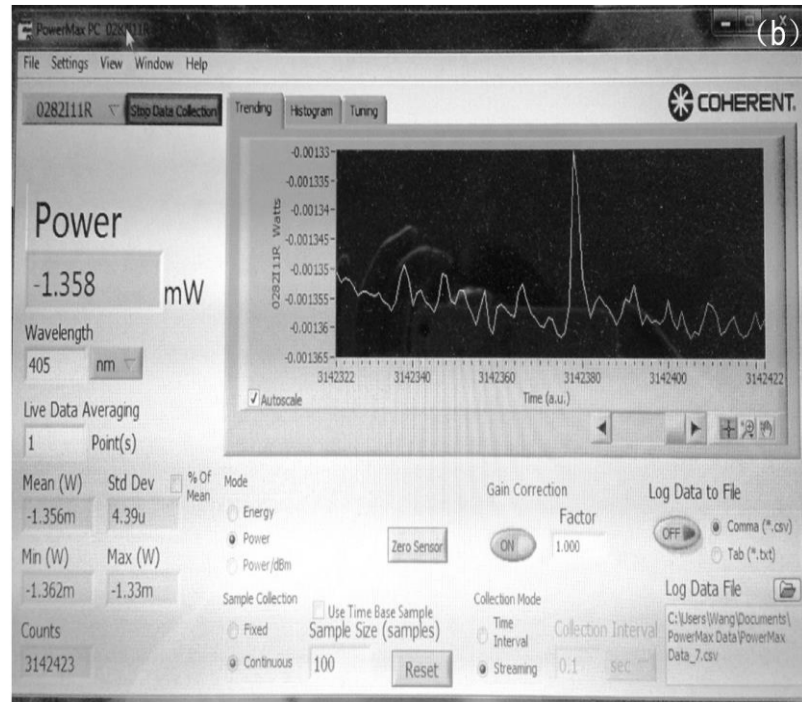| Parameter of PowerMax USB	
Wavelength Range (nm)	300 to 11,000
Power Range	500 μW to 2W
Maximum Thermal Drift (μW)	± 1000
Detector Diameter(mm)	19
Cooling Method	Air
Cable type	USB
Cable Length	2.5m

Figure 2.4 The device to detect the laser power; (a) the model of PowerMax USB; (b) the interface of PowerMax.
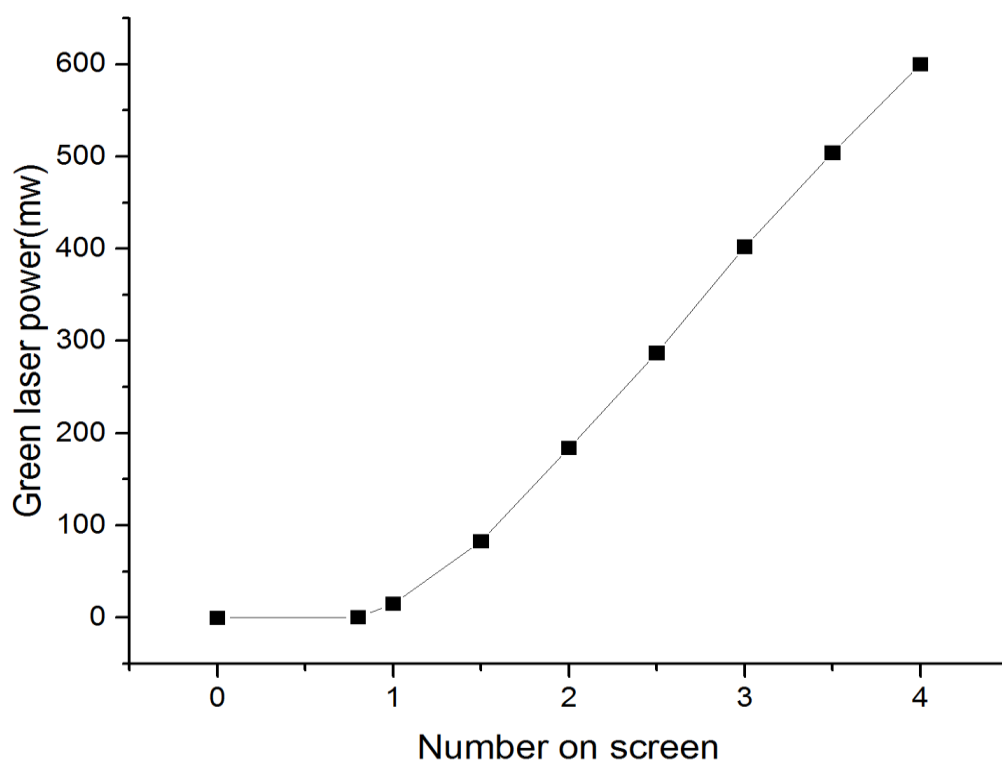
Figure 2.5 the number on screen corresponding with power of green laser.

2.4 THE INTRODUCTION OF NIKON MICROSCOPY AND NIS-ELEMENTS AR

In our experiment, we mainly use Nikon software--NIS-Elements AR. We use this software to combine with the Nikon microscopy (Inverted Research Microscopy ECLIPSE Ti) to scan the specimen. Nikon microscopy is capable of taking on the most advanced bio-science imaging, being an important part of the STED microscopy in our lab. Next, I will introduce Nikon microscopy firstly, then introduce the NIS-Elements AR. The Nikon Microscopy can greatly enhance the scanning speed of STED microscopy to reduce the photo-bleaching largely, because of the following individual motorized components: Nikon-exclusive high-speed encoded stage, Nikon-specified Piezo Z specimen stage, and Nikon filter dichroic cube turret, showing in the Figure 2.6.

The operation and changeover speed of the objectives, X-Y stage, the excitation/barrier filters etc. have been enormously advanced, realizing stress-free operational surrounding that permits research fellows to concentrate on the observations and analysis. We can change the scanning area by controlling the X-Y stage from the four directions and then change the scanning depth of specimen by the Piezo Z stage from the two directions, displaying in the Figure 2.6 (a) and (c). As exhibited in the Figure 2.6 (b), we can flexibly and fleetly change the different objectives.

Nikon microscopy plays a crucial role in our pulsed-STED microscopy. There has another important constituent part - the Nikon's comprehensive imaging software-NIS-Elements AR. The graphical user interface (GUI) of NIS-Elements AR is demonstrated in the Figure 2.7. From Figure 2.7, we can see that the software-NIS-Elements AR can comprehensively control the microscopy, cameras components. The intuitional GUI and effective workflow enable all kinds of functions to be performed easily and to get the automated imaging sequences in 6 Dimensions (X, Y, Z, time, wavelength, multipoint).
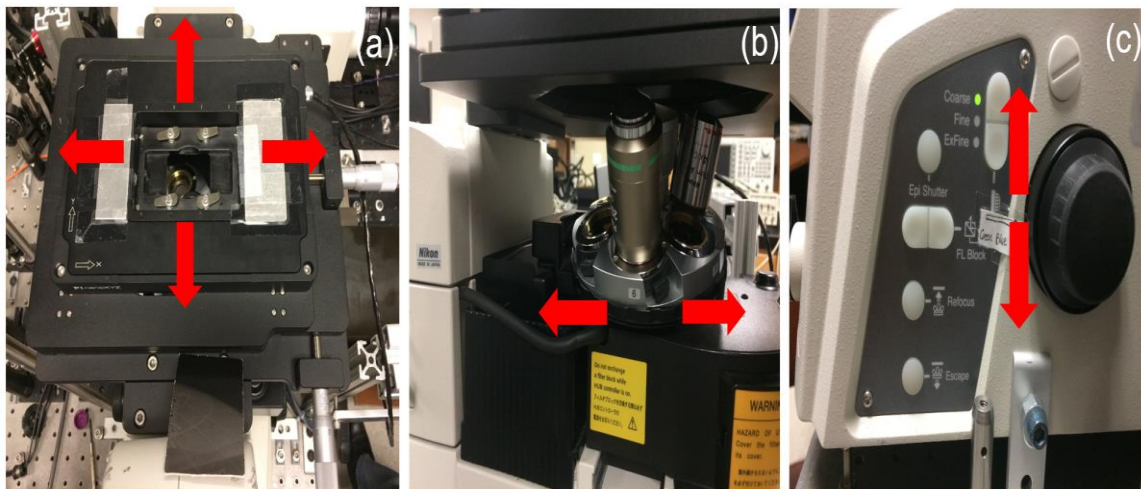

Figure 2.6 Important components of Nikon Microscopy a) Nikon-exclusive high-speed encoded stage; (b) Nikon filter dichroic cube turret; (c) Nikon-specified Piezo Z specimen stage.
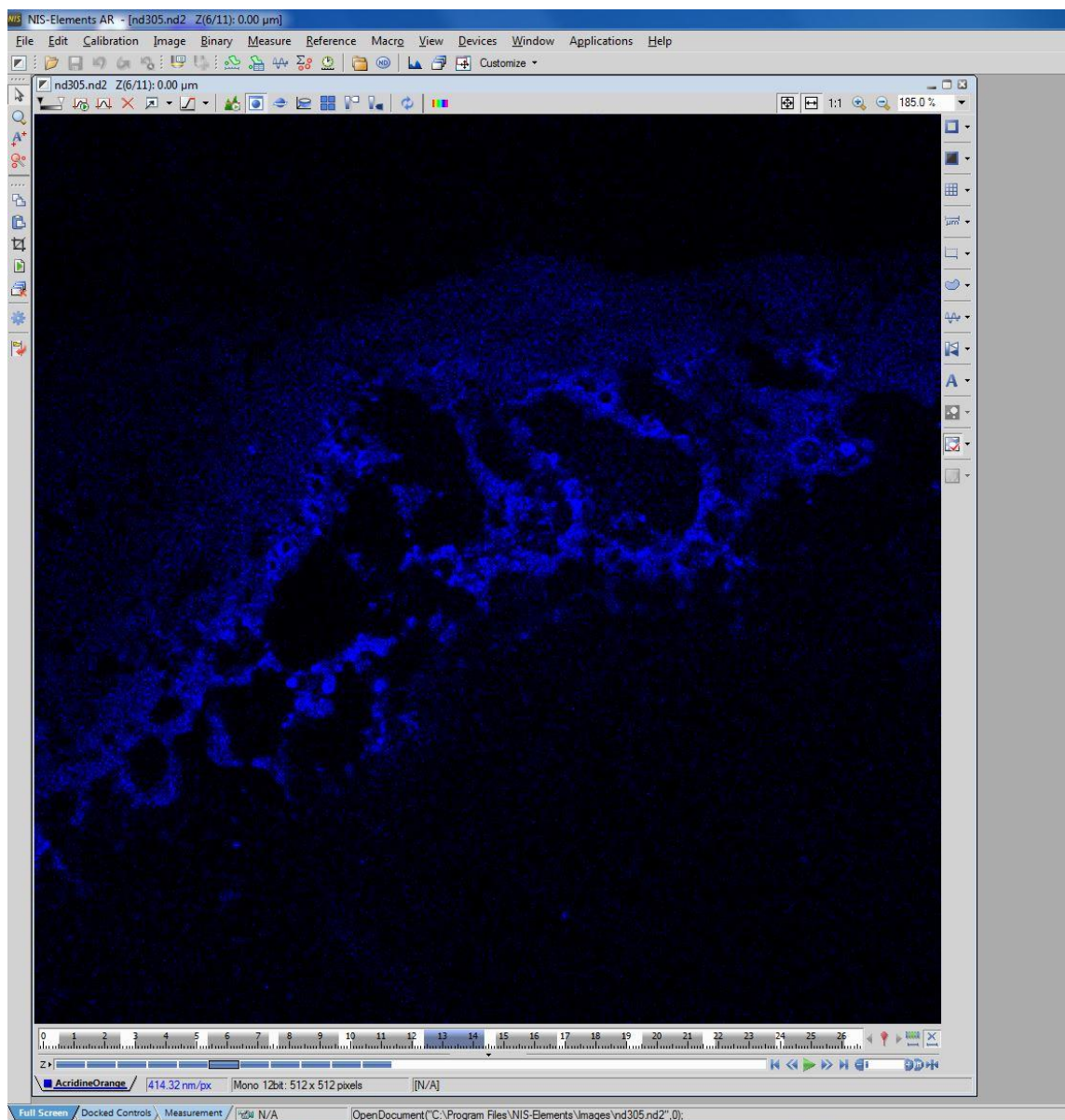
Figure 2.7 The interface of NIS-Elements AR.
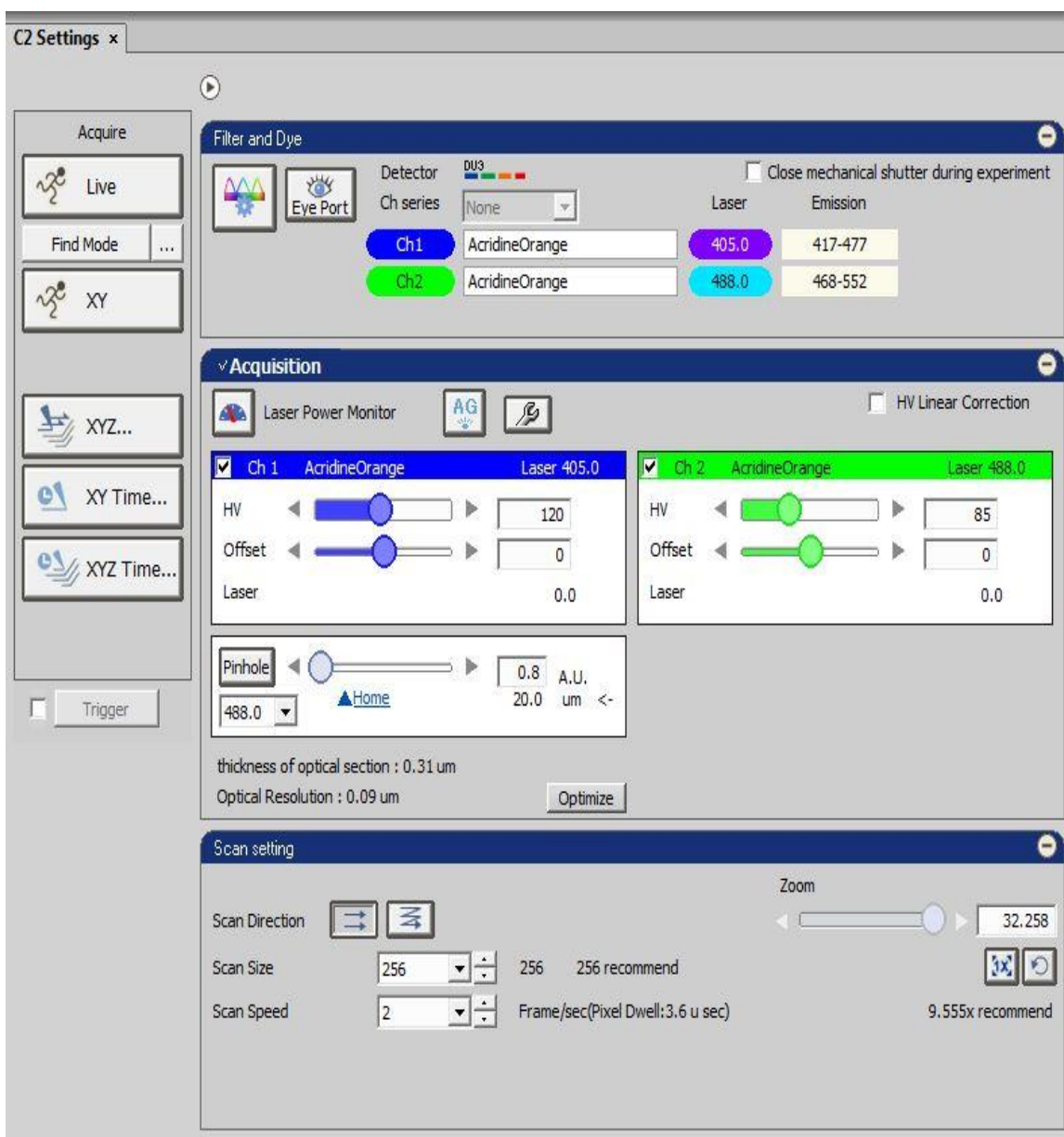
Figure 2.8 The interface of C2 settings.

In our experiment, we mainly use one application of this software to perform the scanning in the C2 setting with changing the size of pinhole, HV, scan direction, scan size, scan speed and even zoom, demonstrating in the Figure 2.8. When the parameters are chosen, we can first click the button "live" to observe the situation of scanning area. Then we can choose different scanning methods, such as 2D-XY and 3D-XYZ.

Additionally, the NIS- Elements AR has various functions to analyz and manage the scanning data, like intensity profile.

2.5 TESTING THE STABILITY AND RELIABILITY OF STED SYSTEM

The excitation and emission spectrums of the dye - Coumarin 102 employed in the experiment can be seen graphically in the Figure 2.9 (a) and the fluorescent signal is shown in the Figure 2.9 (b) by observing in the QImaging QICAM 1394 FireWire Digital CCD Camera. From figure 2.9 (a), we can see that the coumarin is excited maximally at around 412 nm and is emitted maximally at about 470 nm. The certain important points of the laser specifications of the STED system can be observed in purple, green and blue. Furthermore, the wavelength of the excitation beam at approximately 405nm of the STED system is demonstrated by the purple line, closing to the excitation maximum of the coumarin. The green line stands for the STED depletion beam wavelength at near 532nm, which is a little far from the maximal emission wavelength of 470 nm. Because there has an overlap between absorption spectra and emission spectra for ensuring that the depletion wavelength does not disrupt the absorption of coumarin. Set the STED beam wavelength generally to shift toward a little longer wavelength. This is the major reason why choose the wavelength of STED beam with 532nm. The detection range of the STED system is marked in blue rectangle, ranging from 440nm to 490nm, as determined previously by employing the bandpass filters in the overall STED system.
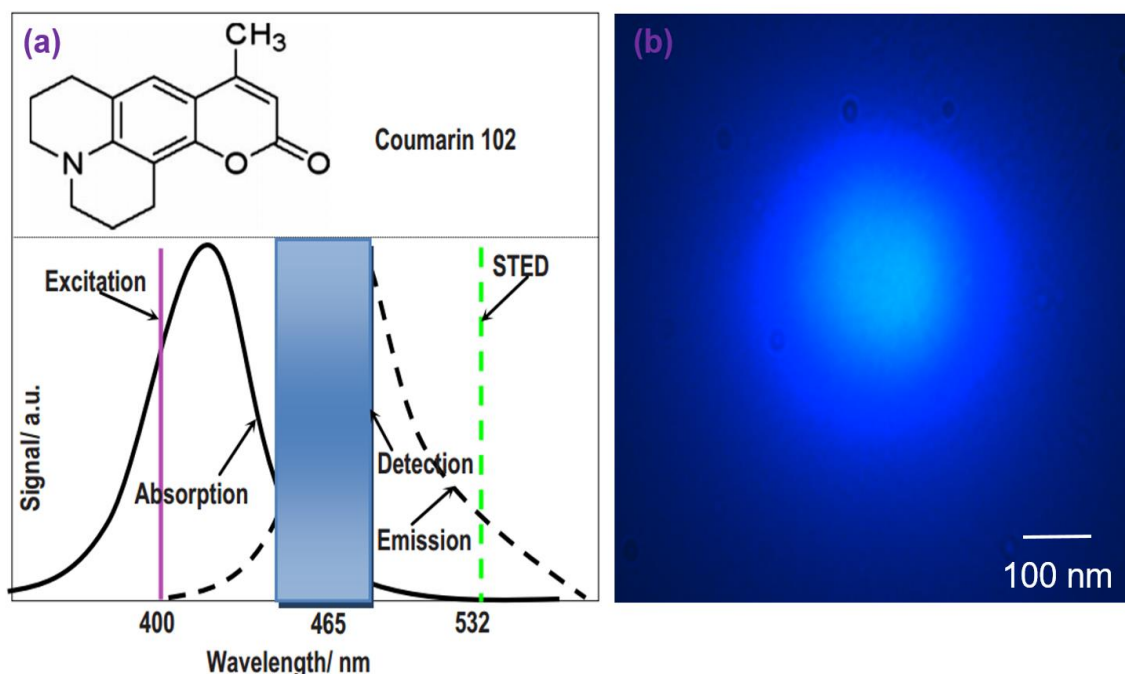
Figure 2.9 (Color online) Optical property of the Coumarin 102 dye. (a) the structural formula of Coumarin 102, excitation and fluorescence spectrum, excitation and STED wavelength, and detection ranges, respectively; (b) The fluorescent signal under the 100 μw UV laser observed in the camera.

The whole process of preparation of coumarin 102 dye is shown in the Figure 2.10. The detailed method is described in the following. We firstly used the electronic scale to weigh the coumarin 102 powder; the weight of coumarin is 146.2mg. And then put the coumarin 102 powder into the test tube, then poured the Ethyl alcohol (50 ml) into the same test tube. Put the cover on the test tube, and then placed the test tube with the coumarin 102 powder and alcohol in the ultrasonic cleaner to shake for 3 minutes. The coumarin 102 would totally solve in the Ethyl alcohol solution after ultrasonic. We could find that the color of the solution from white turning into green, which indicated that we successfully made the 20umol/l coumarin solution.
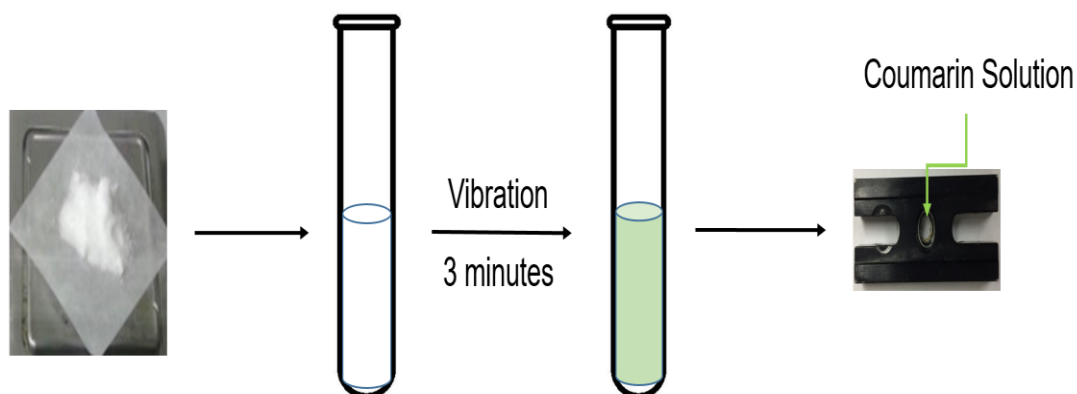
Coumarin 102 (0.15 mg) Ethyl Alcohol (50 ml) Coumarin Solution (20 μmol/l) Reservoir

Figure 2.10 The process to prepare the specimen of coumarin 102 dye.

Finally, took some coumarin solution by the pipette and repositioned them into the reservoir. Lately, we would use the reservoir with coumarin solution to test the stability and reliability of STED system.

In addition, the coumarin solution is very easy to be photo-bleached under light. Therefore, it is important to store the coumarin solution. For our lab, we used the silver paper to warp entirely the test tube of coumarin solution and place them into the freezer.

In this part, we mainly measure the depletion rate of coumarin 102 dye though the STED system we align by ourselves, aiming at verifying the stability and reliability of the system and guaranteeing to high STED resolution for scanning nanoparticles.

The experiment is to validate whether the fluorescent intensity of the coumarin can be depleted by adding the second laser -STED laser or not. In term of the requirements for choosing the dye for STED system, the excitation and emission spectrums of the Coumarin 102 can be applied into STED system. Hence, it normally serves as a sample, using for measuring the depletion efficiency of the system.
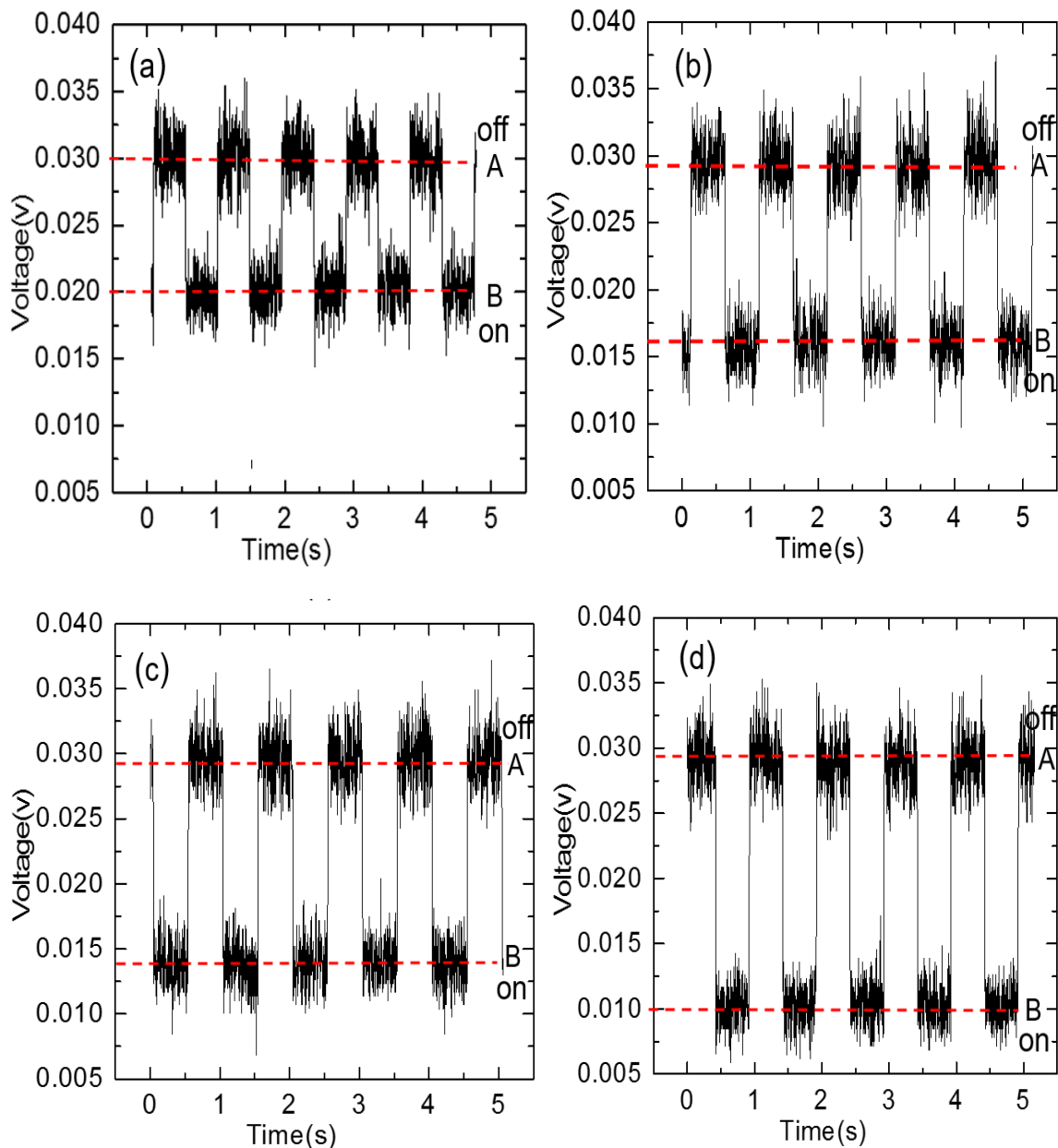
Figure 2.11 Fluorescence intensity using excitation of UV laser of 100 uW and depletion of green laser with various powers: (a) 40mW, (b) 50mW, (c) 83 mW, (d) 235 mW.

To quantitatively analyze the STED depletion measurement on the Coumarin 102 dye, Coumarin 102 was prepared in the water solution, whose concentration is 20 umol. The function generator is applied to control the depletion beam, switching on and off the STED-beam automatically. The depletion rate of fluorescence state was tested in Figure 2.11. As demonstrated in Figure 2.11 (a), depletion efficiencies are displayed by the

36

segments (A) with the depletion beam off and the segments (B) with the depletion beam on. The fluorescent intensity of Coumarin 102 is depleted to different levels corresponding to different powers of the depletion beam. The depletion powers are 40 mW, 50 mW, 83 mW, 235 mW respectively.

From the figure 2.11 (a), there are almost no photo-bleaching under the relatively low power of the excitation beam with 100 uW. Because the signal intensities in the A segment are almost same without the STED laser. We tested the Coumarin 102 when it was in the liquid state. As a result, there probably had a diffusion of Coumarin molecules, passing through the focus spot during the the period of STED laser off. This is due to the new batch of molecules in replacement of partly bleached ones.

From the figure 2.11, we can know that there has a strong reduction in the fluorescence signal when the power of STED laser has a incerease. To more spectific, With increasing power of the cw STED laser beam, the depletion efficiency of Coumarin 102 gradually enhances. Finally, the depletion rate could achieve more than 60% with STED laser power around 235 mW.

In the STED system, the spatial resolution Δr achievable in STED can be defined as $\Delta r \approx \lambda/[2NA(1+P/Psat)^{1/2}]$, where λ is the wavelength of laser, NA represents the numerical aperture of objectives, P denotes the Power of depletion laser, P_{sat} is the effective saturation power for the quenching of the fluorophores used. Based on the equation of resolution Δr, minimizing the wavelength and increasing the ratio of $P/Psat$ can greatly improve the resolution. Therefore, as shown in the figure 2.11, the $Psat$ of the STED is about 77.5 mW, which can be defined as the power at which the probability of fluorescence emission is depleted by half. Hence, it is easier for the ratio of $P/Psat$ to

reach a high value. The experimental results indicate that the STED system we align can work sucessfully and has the potential to achieve a high resolution. The similar experiments have been done by using Atto 390 (SigmaAldrich Corp.) dye, which likewise displays that it has almost the same phenomenon with Coumarin 102 dye.
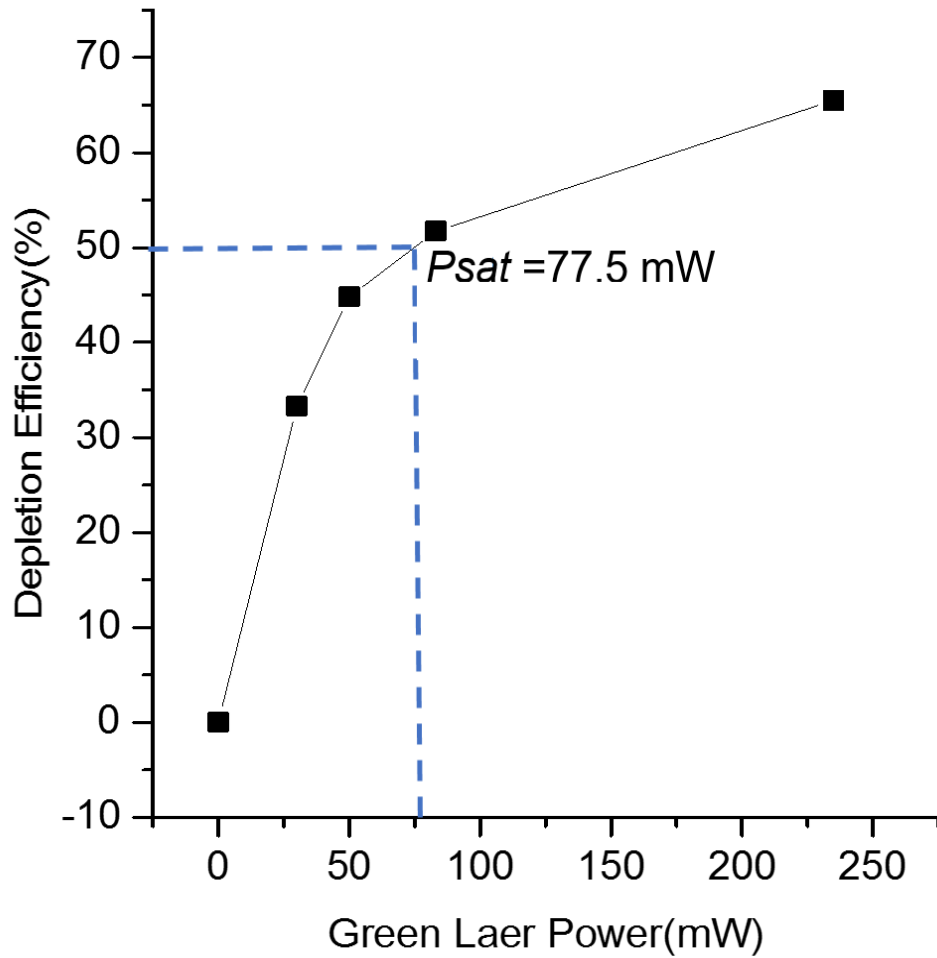

Figure 2.12 STED depletion efficiency as the function of green laser power under excitation of violet laser of 100 µW.

CHAPTER 3

CHOOSING SUITABLE NANOPARTICLE FOR STED SYSTEM

Success in super-resolution imaging depends on the appropriate selection of fluorophores. A broad range of available fluorophores have been developed so far, but not all of them are applicable to STED microscopy. For example, not all dyes can be depleted with a second laser beam. Additionally, fluorophores should have high photo-stability. Therefore, it is highly desired that novel fluorophores can be developed which meet critical requirements for STED applications. The spatial resolution of STED systems can be theoretically described with the following equation:

$$\Delta r \approx \lambda/[2nsin\theta\,(1+P/Psat)^{1/2}] \tag{2}$$

where λ, n, and θ are beam wavelength, refractive index, and half aperture angle of the objective, respectively. P represents the power of the STED beam, and $Psat$ is the saturated power of the depletion beam when fluorescent intensity is half of the maximum. Also, $n\,sin\,\theta = NA$, which denotes the numerical aperture of the objective lens. Based on equation (1), minimizing the wavelength and increasing the ratio of $P/Psat$ are effective ways to improve the resolution. Therefore, discovering new fluorophores with shorter wavelength can enhance the STED resolution. Up to now, much research has been devoted to optimizing the brightness, stability, wavelength and solubility of fluorophores, which can greatly improve the performance of STED microscopy. According to previous reports, many fluorescent dyes have been employed in STED microscopy to obtain a high

resolution, covering wavelengths from 440 nm to 637 nm, including ATTO 633, ATTO 647N, ATTO 590, ATTO 594, ATTO 435 and ATTO 932, etc. For this part of experiment, we focus on the nanoparticles imaging, which will build a foundation for the cell STED imaging.

In the following, we will show how to choose a suitable fluorescent nanoparticle from 3 different kinds of nanoparticle for the STED system imaging based on the data analysis and comparison.

3.1 SPECIMEN PREPARATION OF NANOPARTICLES

In this part, we will choose one kind of nanoparticles which are the most suitable for STED system among three different types of nanoparticles. The three types of nanoparticles are all solutions with high concentration. As a result, the concentration of initial nanoparticle solution is too high for STED system imaging, because if the solution concentration is too high, the fluorescent intensity is very easy to be saturated, and it is very hard to observe the clear pattern of nanoparticles. As shown in the Figure 3.1 (a), we can just see that the whole area full with the blue fluorescent light for light yellow nanoparticle under the lowest excitation power. It is difficult to observe the pattern of signal nanoparticle. Hence, we need to dilute the initial nanoparticle solution into 5 times. The whole process is shown in the Figure 3.1 (b). For solid sample, we used the pipette to extract the initial nanoparticle solution (20 μL) and put it into the test tube with DI water (80 μL). After that, we used the pipette to extract the diluted solution (5 μL) after the diluted solution vibrating 5 mins in the ultrasonic cleaner, and placed the diluted solution on the glass slide. And then, we put the cover slide above the diluted solution. Therefore,

the diluted solution would spread on the glass slide. Finally, we put the glass slide with sample diluted 5 times in the dark place for avoiding the photo-bleaching. When the glass slide totally became dry, which showed that the solid sample diluted 5 times is done.

For the liquid sample, after the diluted solution vibrating 5 mins in the ultrasonic cleaner, use the pipette extract 5 µL and put them into the reservoir. And then use cover slide to cover the reservoir for reducing the evaporation of solution diluted 5 times.
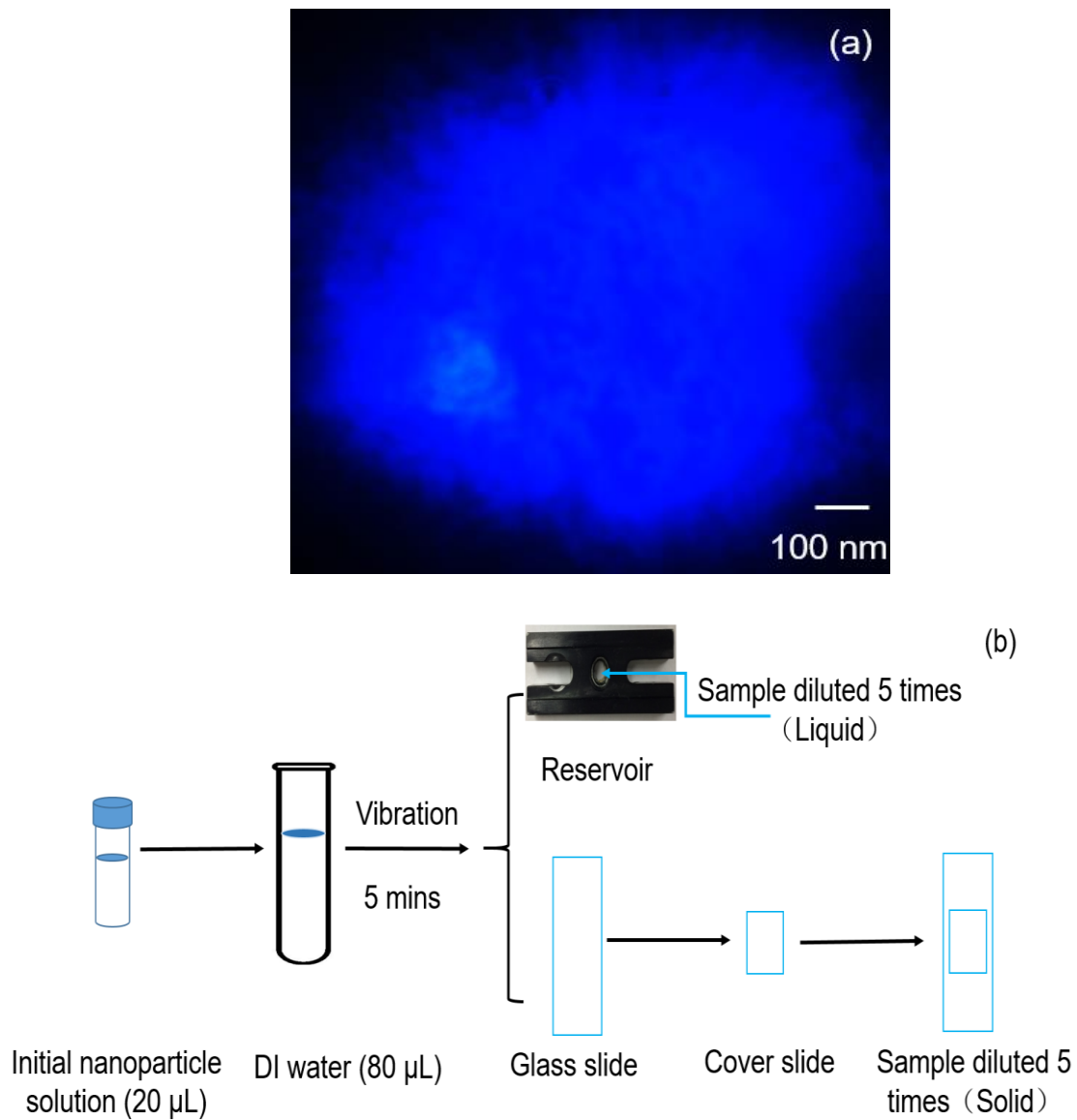

Figure 3.1 (a) The image of light yellow nanoparticle under the lowest excitation power (b) The process to prepare the specimen of nanoparticles.

3.2 OPTICAL PROPERTIES OF FLUORO-MAX BLUE AQUEOUS FLUORESCENT PARTICLES

The first kind of nanoparticle we tried is Fluoro-Max Blue Aqueous Fluorescent Particles (FPs). The size of FPs is 50 nm, which are produced by thermal fisher scientific. The absorption and emission spectrum of the FPs are shown in the Figure 3.1. The absorption intensity of the FPs is very high at the UV wavelength (405 nm). In the emission spectrum of the FPs in Figure 3.1, there has two peaks with 412 nm excitation laser, where the emission reaches its maximum intensity at around the wavelength of 447 nm and 473 nm, respectively. We can clearly observe that the maximal absorption wavelength is at 412 nm and the maximal emission wavelengths are at 447 nm and
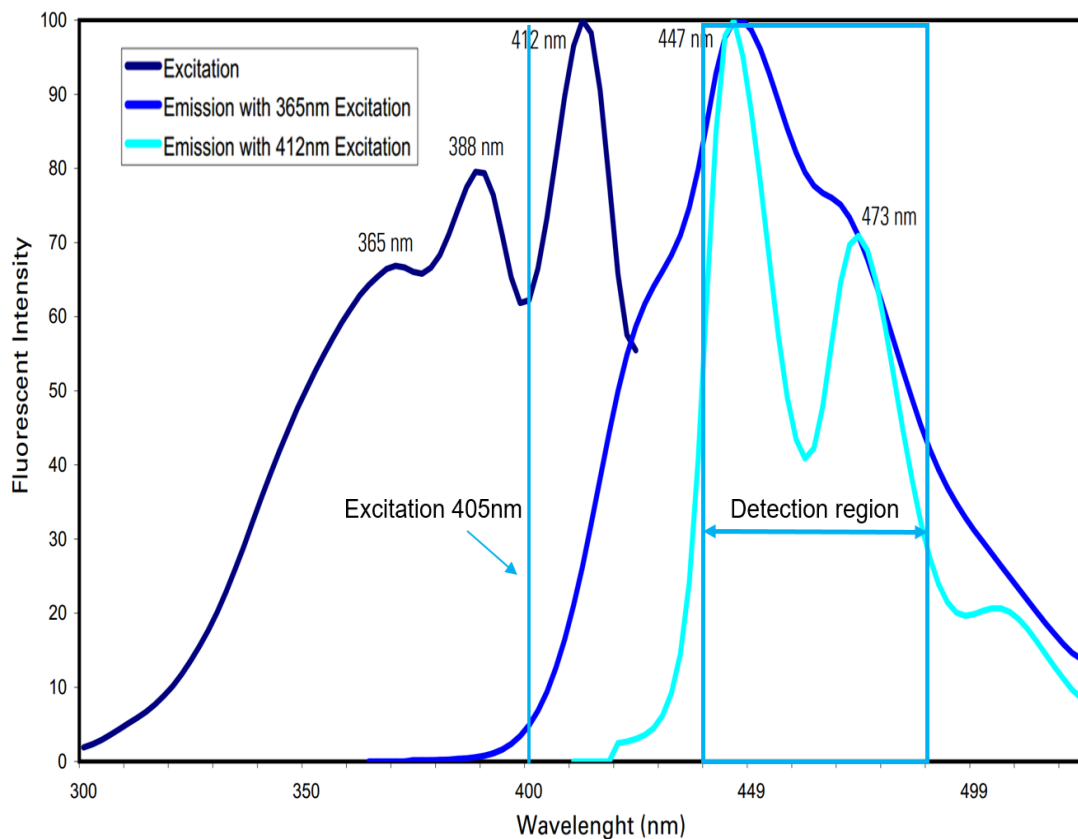

Figure 3.2 Absorption spectrum and emission spectrum of Fluoro-Max Blue Aqueous Fluorescent Particles.

473nm, respectively. More importantly, the excitation laser is 405 nm, with 532 nm

wavelength depletion laser.

To test photo-stability, we measured the fluorescence intensity of the FPs using an

excitation laser power of 100 µW, and the result is illustrated in Fig. 3.3. Remarkably, the

intensity of the fluorescent signal is capable of maintaining itself for a long time (25

seconds) with a stable and steady intensity of approximately 0.16 V when the excitation

laser is on, demonstrating an outstanding photo-stability. The fluctuation around 0.16 V is

due to the shot noise of the detector. When the excitation laser is turned off, the

fluorescence intensity becomes approximately background noise level, i.e. about only

0.01 V low for wavelength around near 532 nm. The FPs still could be a potential
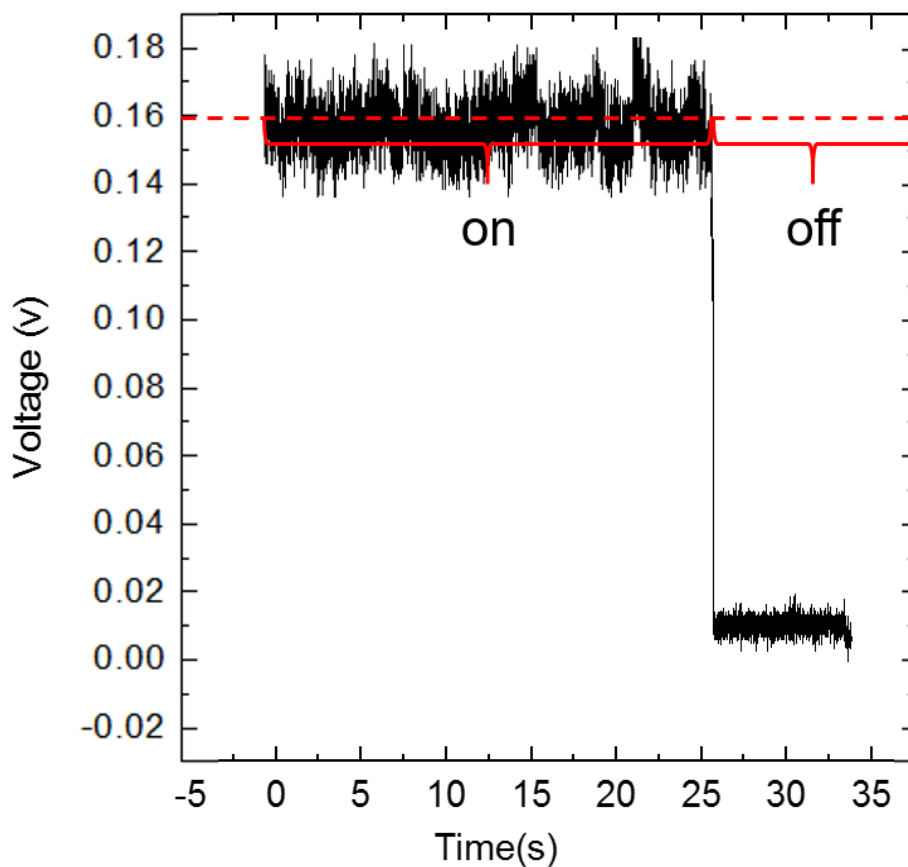

Figure 3.3 Photo-bleaching of FPs in STED system under the 100µw excitation laser.
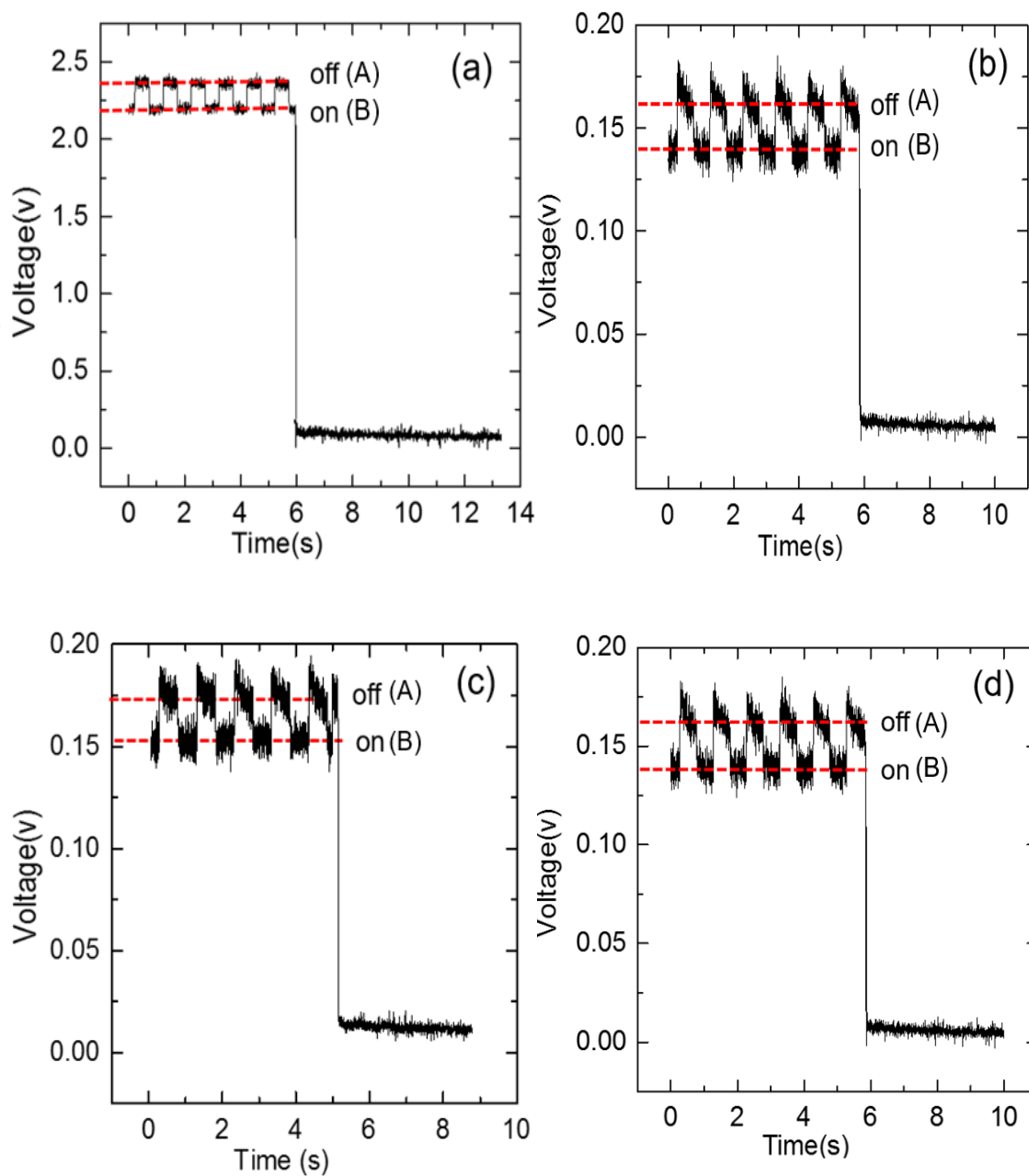
Figure 3.4 Fluorescence intensity using excitation of UV laser of 100 µW and depletion of green laser with various powers: 287 mW, 402 mW, 502 mW and 600 mW

candidate for STED system, despite that the fact is that we cannot make sure if the absorption intensity of the FPs. Therefore, we further detect the depletion efficiency of FPs. For the laser depletion test, we used a function generator to control and synchronize the laser beams on and off. When the function generator is used to control the depletion beam on and off, the depletion rate of the fluorescence state can be measured. As shown in Figure 3.4, depletion behavior is displayed by showing segment (A) with the depletion beam off and the segment (B) with the depletion beam on. The fluorescence intensity of the FPs is depleted to different levels corresponding to the different powers of the depletion beam. In Figure 3.4, the depletion powers are 287 mW, 402 mW, 502 mW and 600 mW, respectively, with the corresponding depletion efficiencies are of 8.5% ,12.5%,14.3% and 17.6%.

From the Figure 3.4, we can observe that photo-bleaching is very low, because the fluorescent intensity always can recover to the original value after a short period of depletion laser on. For this point, the FPs is a good candidate for STED system imaging. Accor to the equation (2), the depletion rate had better reach 50% when *Psat* is really low. But, for the FPs, the highest depletion rate only can reach 17.6% when the power of STED laser achieves 600 mW, showing that the depletion effect is not obvious. In summary, the FPs are not good enough for STED system imaging.

3.3 THE OPTICAL PROPERTIES OF SILICA NANOPARTICLES-NFv465

The second one we tried is the NFv465 (20nm, ACZON S.r.l.), which absorbs in the violet part of the spectrum (the maximum wavelength of absorption 420nm) and emits in the blue part of the spectrum (the maximum wavelength of emission 467nm), showing in the Figure 3.5. We can see that the absorption intensity of the NFv465 is very high at

the UV wavelength-405 nm. Then, the absorption first increases to a maximum at about

420 nm, and then decreases sharply again until 500 nm. Especially, the absorption of the

NFv465 is almost zero around the wavelength near 532 nm in the absorption spectrum. In

the emission spectrum of the NFv465 in Figure 3.5 (b), there is a peak, where the

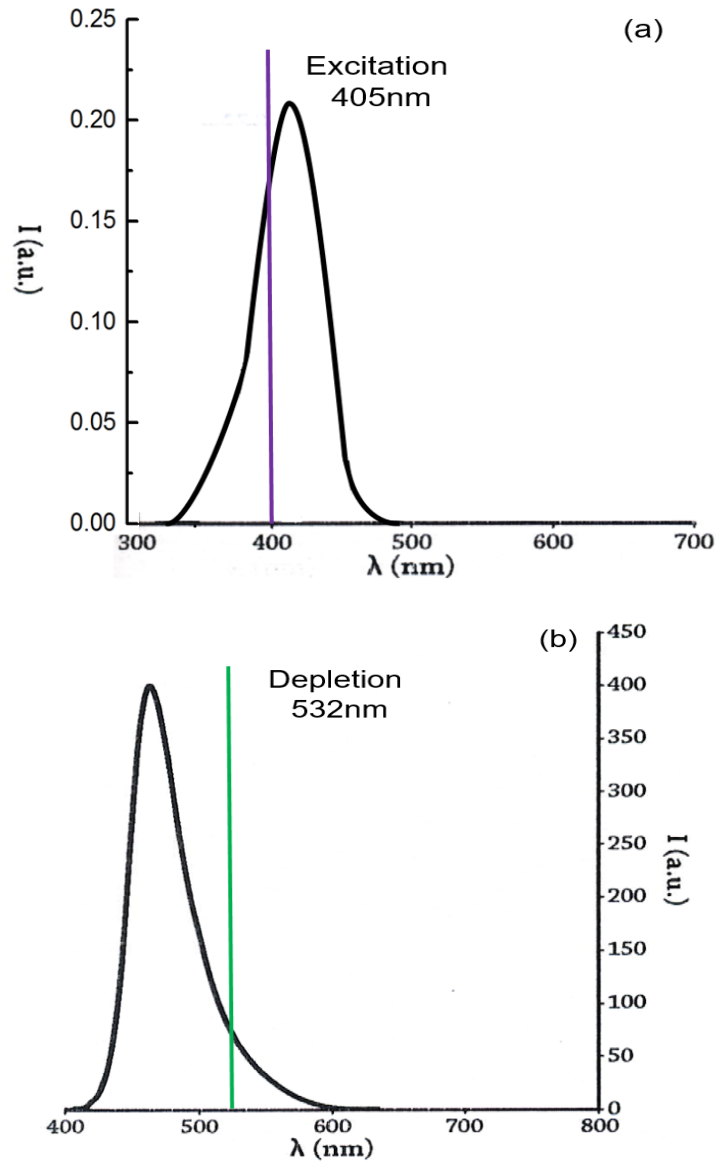emission reaches its maximum intensity at around the wavelength of 467 nm. There still

Figure 3.5 Spectra of NFv465: (a) absorption spectrum and (b) emission spectrum.

has certain intensity when the wavelength is near 532 nm. More importantly, the Stokes shift of the NFv465 is 47 nm, which means the NFv465 can effectively avoid self-absorption and causing background interference. Figure 3.5 (a) also demonstrates that the absorption intensity of the NFv465 is almost zero for the wavelength around 532 nm. This indicates that the NFv465 can be excited by the excitation laser (405 nm), and depleted by 532 nm wavelength simultaneously.

The concentration of the NFv465 is 0.54 mg/ml. Then, I detected the photo-bleaching and the depletion rate of NFv465 nanoparticle in the STED system. The photo-bleaching results are showed in the Figure 3.6. From the Figure 3.6, we can observe that the fluorescent intensity of NFv465 nanoparticle is near 0.1 v at the beginning, then the fluorescent intensity gradually decreases.
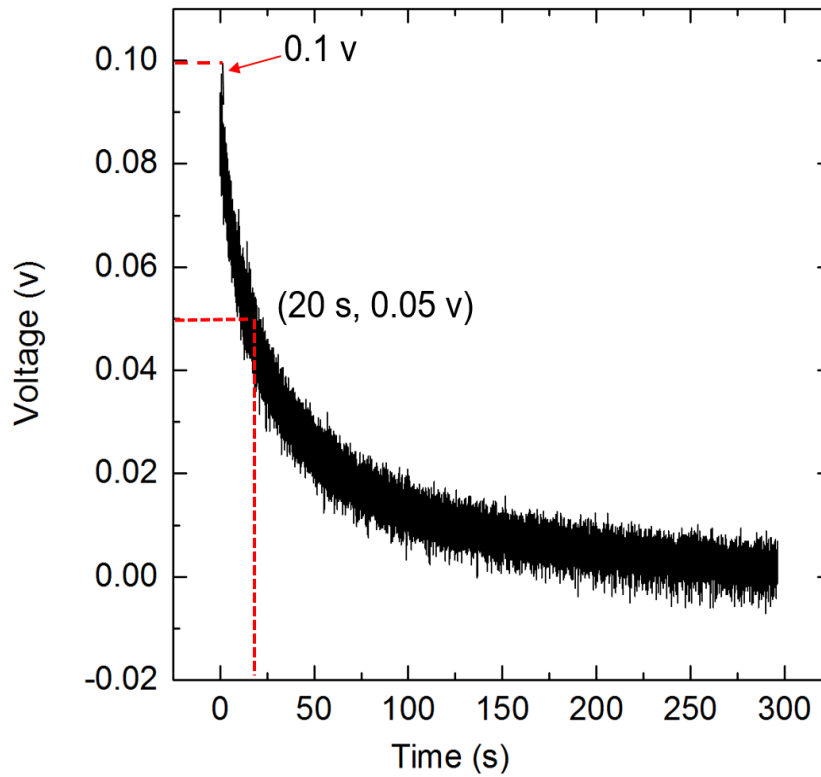

Figure 3.6 Photo-bleaching of NFv465 in the STED system under the 100 μW excitation laser.

When the time is approximately 20 s, the fluorescent intensity of NFv465 nanoparticle become half of the initial fluorescent intensity, which display that the photo-bleaching of nanoparticle NFv465 is not serious under excitation laser. Therefore, nanoparticle NFv465 meets the following criterion: the NFv465 can be excited by the excitation laser (405 nm), and depleted by 532 nm wavelength simultaneously. And the photo-bleaching of NFv465 is low. These all indicate that the present NFv465 could be a very useful nanoparticle candidate for STED system imaging. The depletion efficiency of NFv465 under the excitation laser power (100uw) and different green laser power is shown in the Figure 3.7. Firstly, we can observe that the photo-bleaching is very serious in the Figure 3.7 (a), (b), (c) and (d). Even though the depletion power is very small (50mw, 83mw), the photo-bleaching is still high. What's worse, there is almost no depletion efficiency, demonstrating in the Figure 3.7 (a) and (b). When the depletion power increases, the depletion efficiency also has an enhance.

Nonetheless, the photo-bleaching is still high. As displayed in the Figure 3.7 (c) and (d), the depletion efficiency is 37.5% and 43.2%, with the corresponding depletion lasers which are 287 mw and 402 mw. Herein, NFv465 is not an ideal candidate for our STED system imaging, due to the high photo-bleaching and low depletion efficiency.
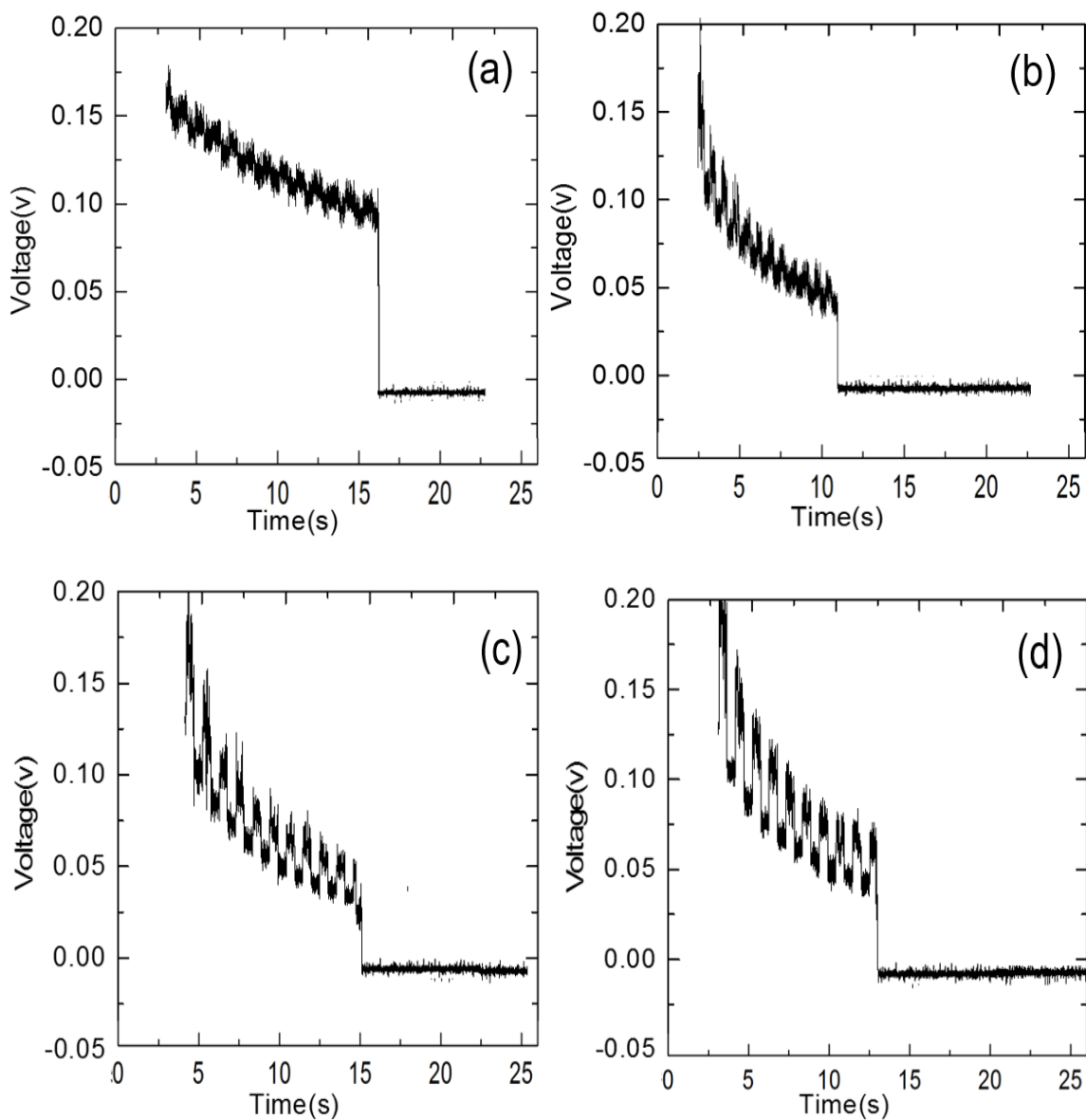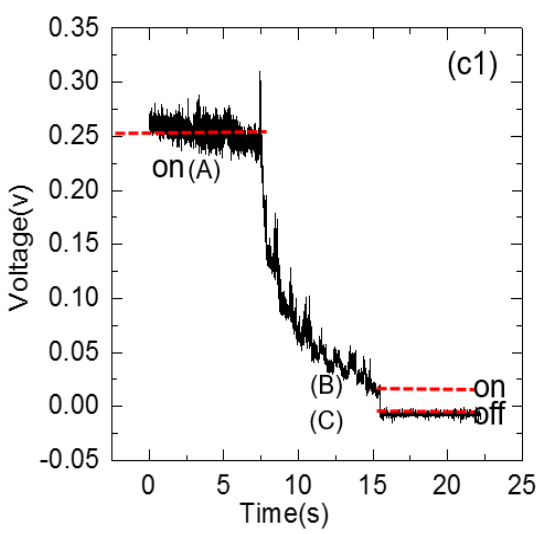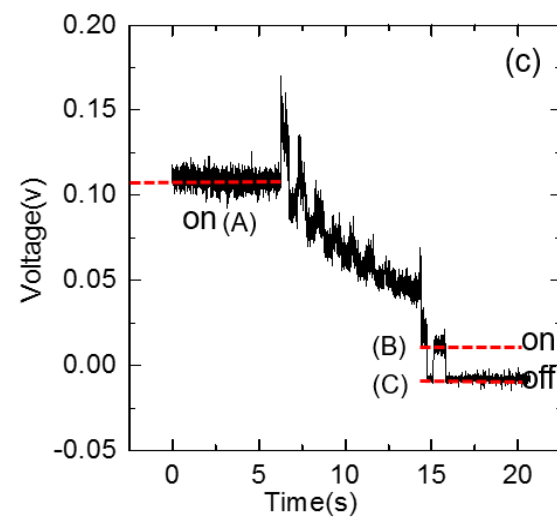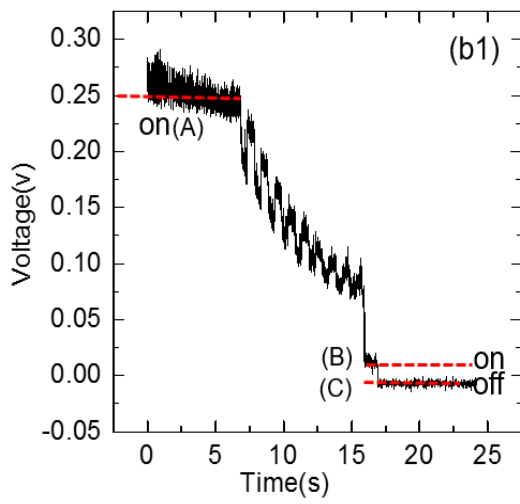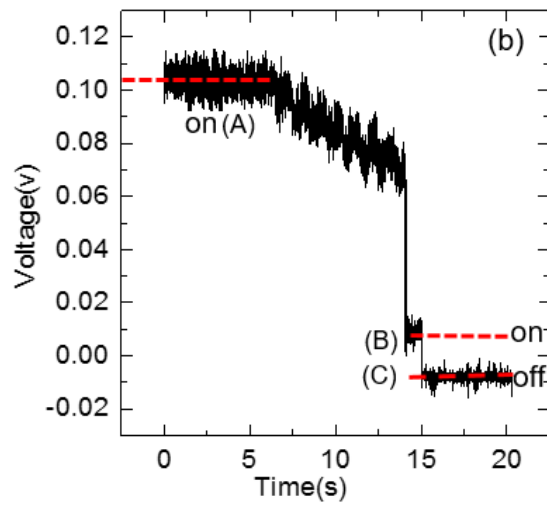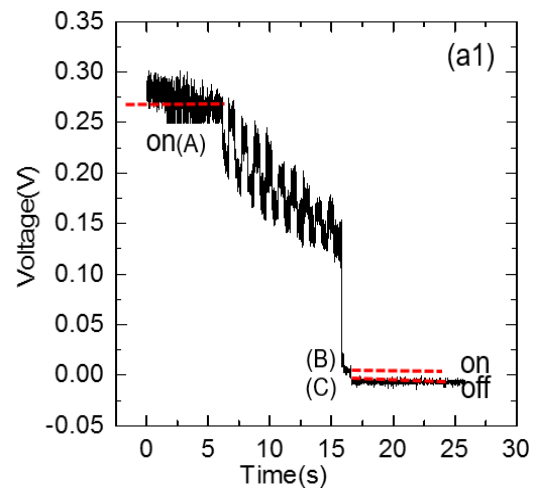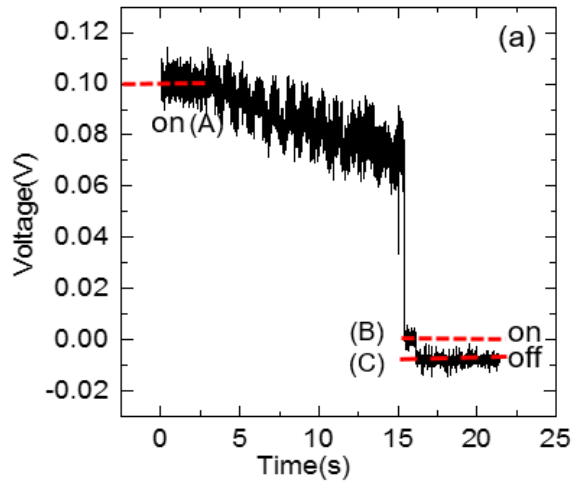
Figure 3.7 Fluorescence intensity using excitation of UV laser of 100 µW and depletion of green laser with various powers 100 µw and depletion of green laser with various powers: (a) 50 mW, (b) 83 mW, (c) 287 mW, (d) 402 mW.

For the nanoparticles NFv465, we also measure the depletion efficiency under the solid and liquid state. For this experiment, we started to record the signal intensity at the beginning when only excitation laser is on, instead of recording the signal intensity with the excitation and depletion laser on. We can notice that there have a lot of differences for the nanoparticles NFv465 between the liquid and solid. In each image of the Figure 3.8, the segment (A) means that the NFv465 emitted fluorescence when the excitation laser was on. It is pretty evident that the intensity is much higher in the solid than in the liquid. The fluorescent intensity is always near to the 0.10 V in the liquid situation, showing in the Figure 3.8 (a), (b), (c), (d) and (e). Meanwhile, as shown in the Figure 3.8 (a1), (b1), (c1), (d1) and (e1), the fluorescent intensity always has a little fluctuation near 0.25V. In addition, the depletion efficiencies in the liquid state are 13.5%, 13.6%, 25.7%, 32.1%, 38.5% respectively, with corresponding depletion powers which are 50 mw, 83 mw, 200 mw, 287 mw, and 400 mw. But when the depletion powers are under 50 mw and 83 mw, the corresponding depletion efficiencies are only19.5% and 25.9%. Furthermore, under the other depletion powers (200 Mw, 287 Mw and 400 Mw), we even cannot calculate the corresponding depletion efficiencies due to the serious photo-bleaching effect of depletion laser.

Hence, we can conclude that the depletion rate is higher in the liquid state and the photo-bleaching is also less serious than that in the solid state. Especially, the photo-bleaching is extremely serious in the Figure 3.8 (e1), when the power of depletion laser is
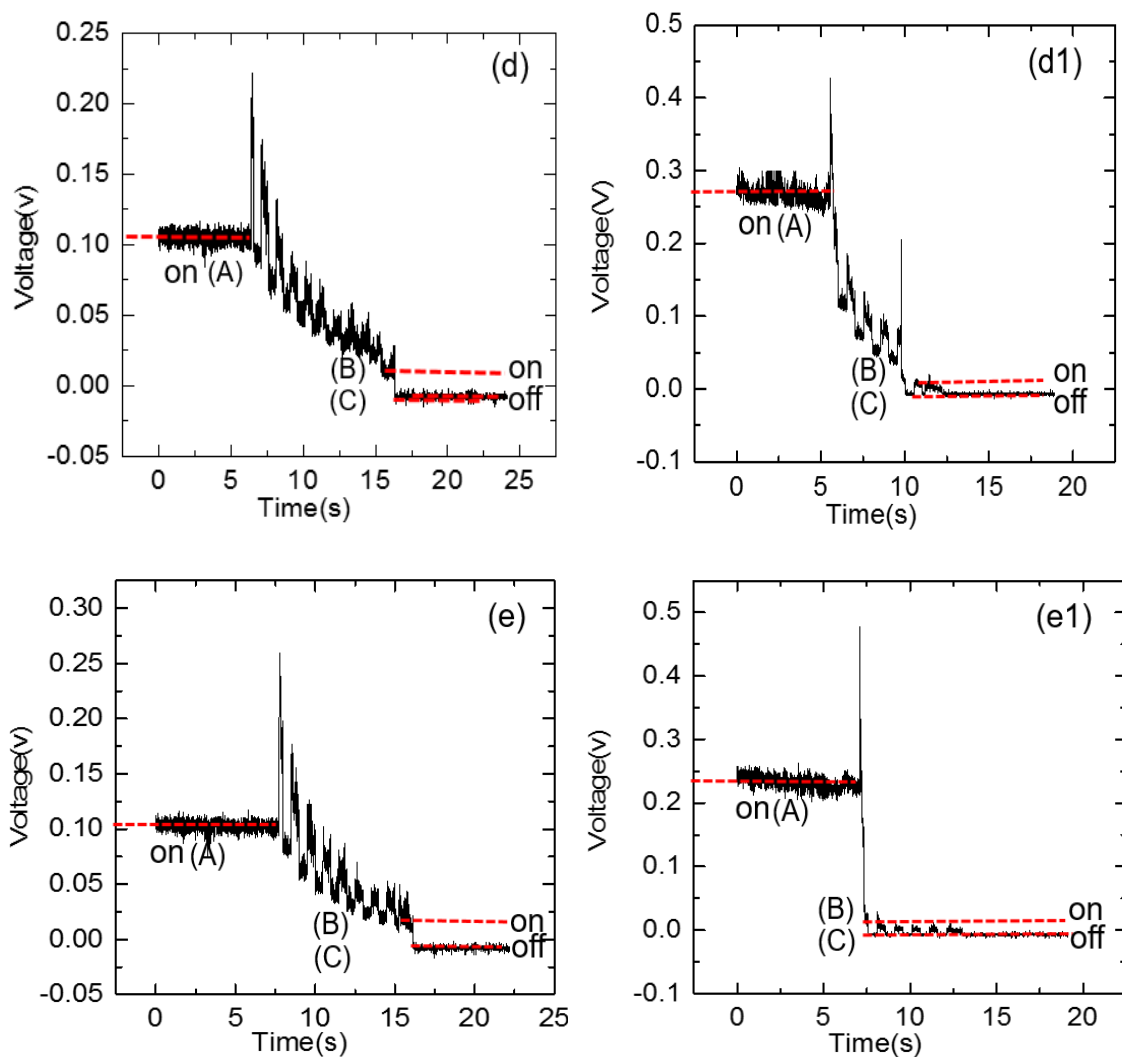
Figure 3.8 Fluorescence intensity using excitation of UV laser of 200 μW and depletion of green laser with various powers: (a) and (a1) 50 mW, (b) and (b1) 83 mW, (c) and (c1) 200 mW, (d) and (d1) 287 mW, (e) and (e1) 400 mW; (a), (b), (c), (d) and (e) in the liquid state;(a1), (b1), (c1), (d1) and (e1) in the solid state.

400 mw. One reason why the photo-bleaching is lower in the liquid state is that the liquid can flow, so the photo-bleaching part is easily replaced by the new sample without photo-bleaching. In the Figure 3.8, the segment (B) means that the excitation laser is off and the depletion laser is on. And then the segment (C) means that both the excitation laser and depletion laser are off. Additionally, there still has the fluorescent intensity in both solid and liquid states when only depletion laser is on. This illustrates that the NFv465

also absorbs the light of the depletion laser (532 nm). Besides, the fluorescent intensity decrease greatly, even when the depletion laser is low in both situations, showing in the Figure 3.8 (a), (a1), (b) and (b1). Nonetheless, the fluorescent intensity suddenly has an increase when the depletion laser become larger in liquid and solid states, displaying in the Figure 3.8 (c), (c1), (d), (d1), (e) and (e1). We can conclude that when the depletion laser increase to certain level, the depletion laser cannot deplete the fluorescent intensity of NFv465 and even could enhance the signal intensity of the NFv465.

3.4 OPTICAL PROPERTIES OF LIGHT YELLOW NANOPARTICLES

The third kind of nanoparticle we tried is light yellow nanoparticles (LYs,100nm, Spherotech). The excitation spectrum of LYs is displayed in the Figure 3.9. We can see that when we use 405 nm laser to excite the LYs, the LYs can emit an extremely high intensity. And the emitting intensity is extremely low when the wavelength is near to 532 nm. Even though we lack the emission spectrum of LYs, the LYs still is possible to be an ideal candidate for STED system. We did the following experiment to test the optical properties of LYs.

Firstly, we measure the photo-bleaching of LYs to observe if the signal intensity is stable or not. The result is shown in the Figure 3.10. From the Figure 3.10, we can observe that the fluorescent intensity of LYs nanoparticle is near 0.10 v at the beginning, then the fluorescent intensity gradually decreases.
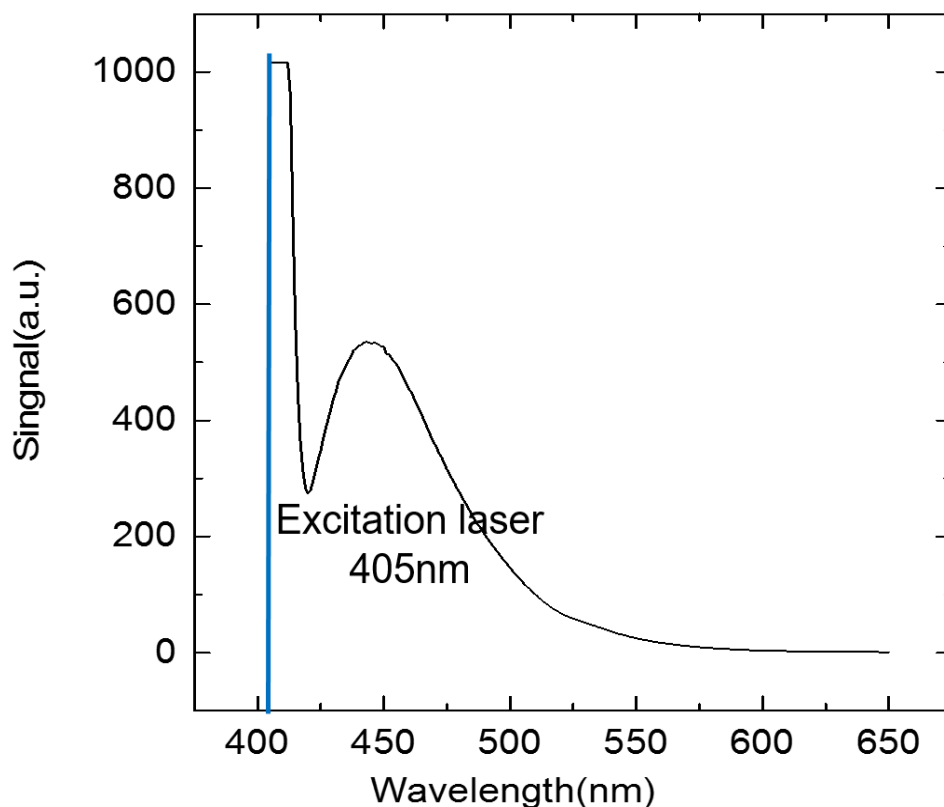
Figure 3.9 Absorption spectrum of LYs.

When the time is approximately 45 s, the fluorescent intensity of LYs

nanoparticles becomes half of the initial fluorescent intensity. Furthermore, the

fluorescent intensity of LYs takes about approximately 400 s to become zero. These

results display that the photo-bleaching of LYs is not serious under 100 μw excitation

laser. Then we detected its depletion efficiency, demonstrating

in Figure 3.10, depletion behavior is displayed, showing in the segment (A), (C), (E) and

(G) with the depletion beam on and the segment (B), (D), (F) and (H) with the depletion

beam off. The fluorescent intensity of the LYs is depleted to different levels

corresponding to the different powers of the depletion beam. The original intensity of

LYs is 0.104 V when only excitation laser is on, then the fluorescent intensity decreases

largely when the excitation laser and depletion laser are both on ((A), (C), (E) and (G) and then the depletion laser is off ((B), (D), (F) and (H)). The fluorescent intensity has an increase when the depletion laser is off, but the intensity is lower than the original value, revealing that there has a photo-bleaching under the both laser and not serious in a short time. In Figure 3.11, the depletion powers are 40 mW, 83 mW, 184 mW and 402 mW,
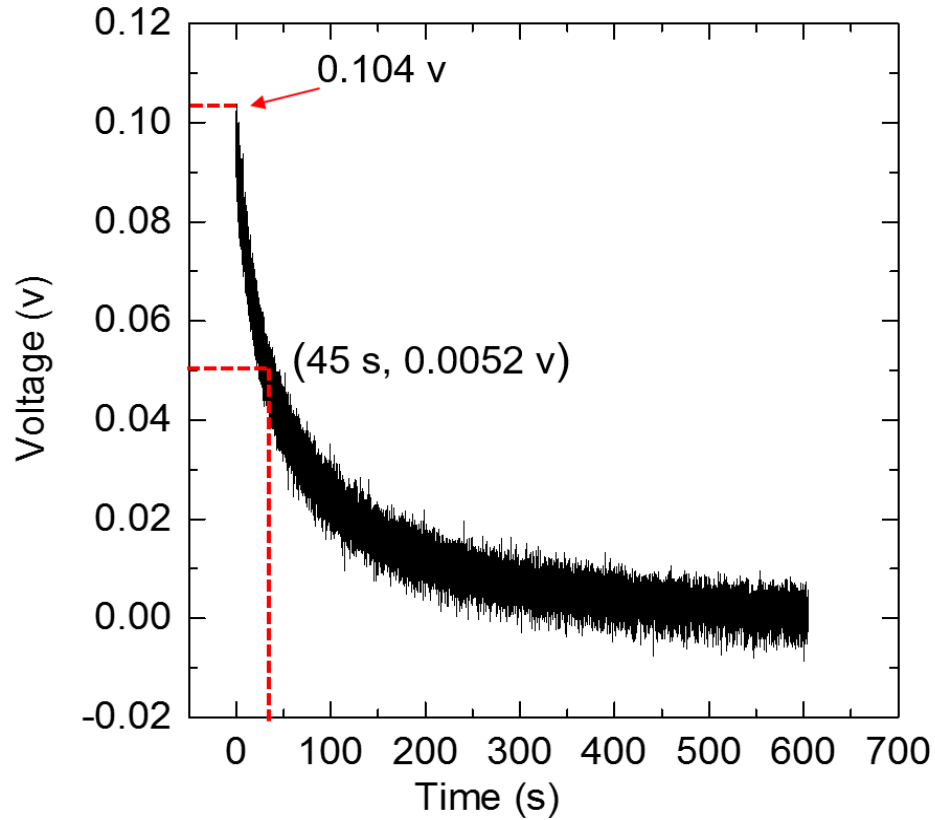
Figure 3.10 Photo-bleaching of LYs in the STED system under the 100μw excitation laser.

respectively, with the corresponding depletion efficiencies which are 31.4%, 38.1%, 47.6% and 61.9%. These results show that the depletion efficiency is high, even under the low depletion power. In despite of the little high photo-bleaching of LYs, the LYs are still an ideal candidate for STED with high depletion efficiency.
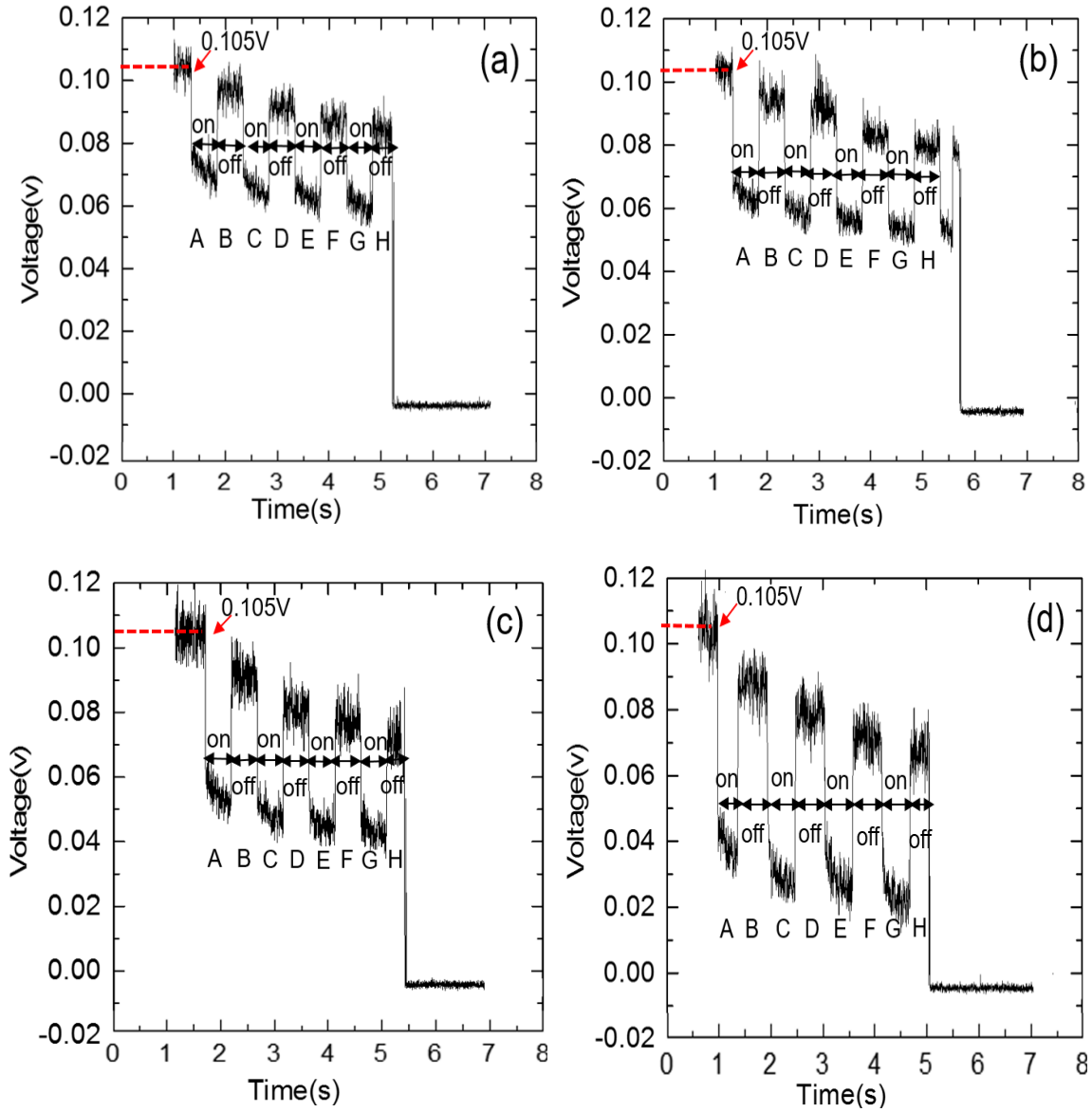
Figure 3.11 Fluorescence intensity using excitation of UV laser of 100 μw and depletion of green laser with various powers: (a) 40 mW, (b) 83 mW, (c) 184 mW, (d) 400 mW.
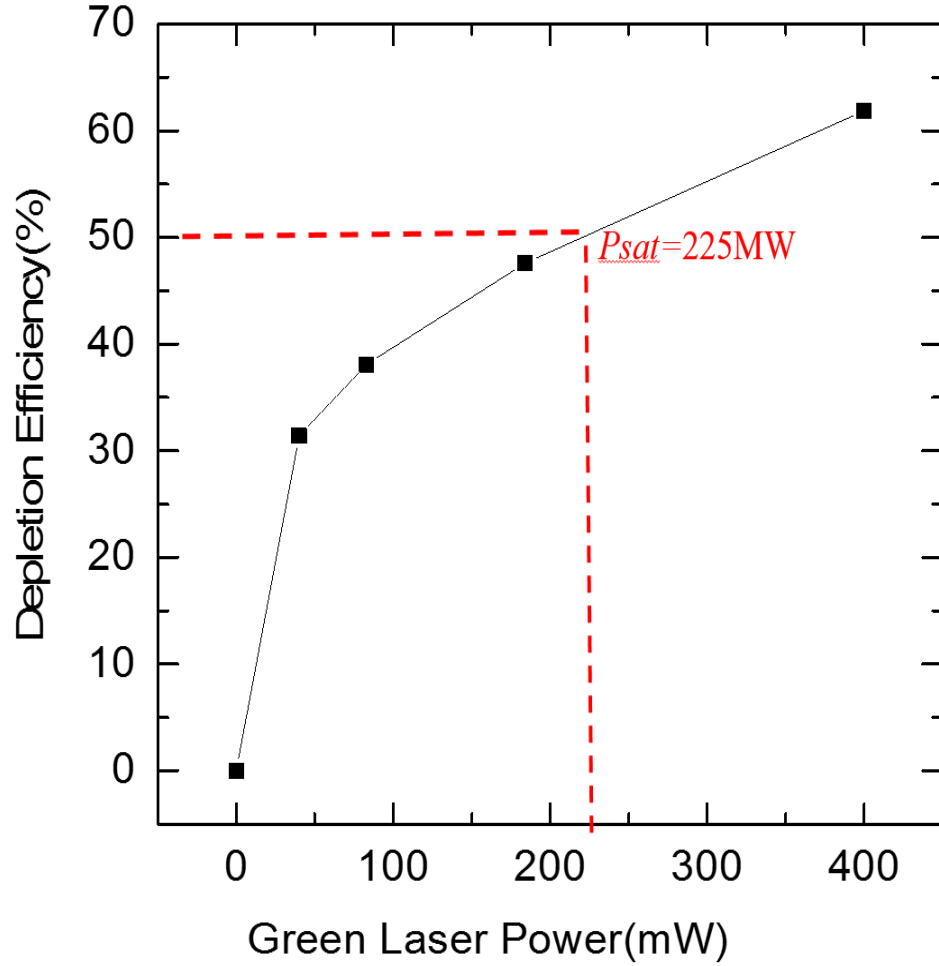
Figure 3.12 STED depletion efficiency as the function of green (depletion) laser power under 100 μW UV laser.

In order to evaluate the potentially achievable spatial resolution when LYs are used in STED microscopy, the relationship between the depletion efficiency and the power of the depletion laser of the LYs is presented in Figure 3.12. It reveals that the larger the power of the depletion laser, the higher the depletion efficiency would be. From the curve in Figure 3.12, we can calculate that the *Psat* of LYs is equal to 225 mW when the depletion efficiency achieves to 50%.

According to the equation (1), the increase of the resolution relies on the intensity or the power of the depletion beam in the STED system. To be specific, maximizing the

square root of the saturation factor *P/Psat* can greatly improve the STED resolution. Therefore, the LYs have the potential to improve greatly the resolution of STED system.

The image of LYs is observed in the camera, showing in the Figure 3.13. On the one hand, we could clearly observe the pattern of nanoparticle by camera, and the fluorescent intensity is also very strong under the excitation laser with 100 μw, which can help us make sure the scanning area for the STED system imaging. On the other hand, observing from camera can help us make sure the value of power of excitation laser. The fluorescent intensity will increase when the power of the excitation laser is larger. If the fluorescent intensity is too larger, the intensity will be saturated, then it will become hard for us to observe the pattern of specimen. We need to change the power of the excitation laser until that we could get an ideal and clear pattern in the camera.
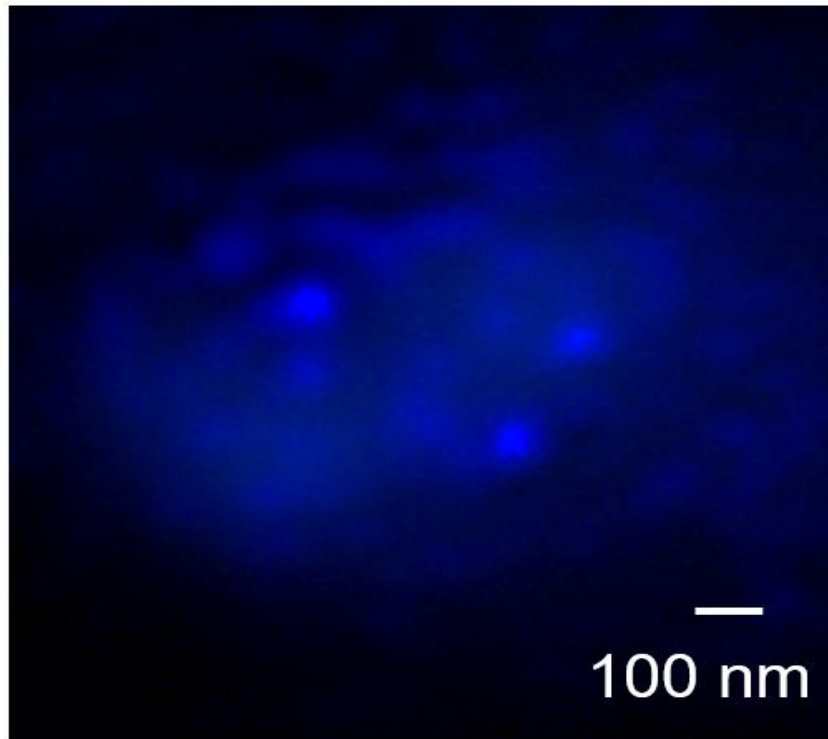
Figure 3.13 The pattern of nanoparticle observing by the camera under the excitation laser with 100 μW.

3.5 SUMMARY

Comparing to the three types of nanoparticles (FPs, NFv465, LYs), the LYs are the most suitable for our STED system. The reasons are in the following. For the FPs, the fluorescence intensity is strong and extremely stable. The photo-bleaching is low and not serious, because the fluorescence intensity can always go back to the original value after the depletion laser on. However, the obvious disadvantage is that the depletion laser does not have an obvious depletion effect, due to the slight depletion efficiency. For example, when the power of the depletion laser is 600 mw, the depletion rate can only reach to 17.6%.

For the NFv465, this kind of nanoparticle is still good enough for our STED system. Even though that the photo-bleaching is not serious only the under the excitation laser, the photo-bleaching become a little serious under the depletion laser. What's worse, the depletion effect of depletion laser is extraordinarily low because we hardly calculate the depletion rate when STED laser is small (50 mw, 83 mw). When the depletion laser becomes larger, the depletion rate gradually becomes higher. The photo-bleaching is extremely serious. Therefore, the NFv465 is still not a good choice for our STED system.

For the LYs, we finally choose this one as our ideal nanoparticles for our STED system. Despite of the photo-bleaching under the excitation and depletion laser, the depletion effect is highly obvious, when the depletion laser is 40 mw, the depletion efficiency could reach 31.4%. Especially, when the depletion laser achieves to 400 mw, depletion efficiency could attain to 61.9% with that the photo-bleaching is acceptable.

CHAPTER 4

RESULT AND DISSCUSION

4.1 IMAGES OF STED MICROSCOPY

In the end, we employed the pulsed-STED setup to obtain the nanoscale imaging of light yellow nanoparticles (LYs, spherotech) according to the analysis of Chapter 3. The solid specimens of LYs were prepared via using the approach explained in the Chapter 3. A dilute dispersion of 100 nm LYs beads prepared by drop-casting the solution of the nanoparticle on a glass slide and a coverslip, and the specimen was scanned by utilizing the different STED parameters. The excitation and STED wavelengths are (405) nm and (532) nm, respectively; the other conditions are in the followings: the position of excitation laser power is at 235, we can adjust the value of the power by changing the position. The STED beam had approximately 20mW of optical power at the front aperture of the objective lens. And the pinhole size was 20μm, the PMT HV was about 140V (no linear correction and offset=0), the scan size was 512 *512 pixels, the scanning speed was 1/8, and the zoom was 16, as displayed in the Figure 4.1. The X, Y and Z positions were 8.94 mm, 12.042 mm and 4499.9 μm respectively.

In order to make a comparison, the Confocal and STED images of the LYs were performed in STED and confocal modes, shown in Figure 4.2 (a) and (c), respectively. The nanoparticles in the confocal image are a little blurred, whereas more single nanoparticles could be brought out in the STED counterpart. The confocal image (Figure
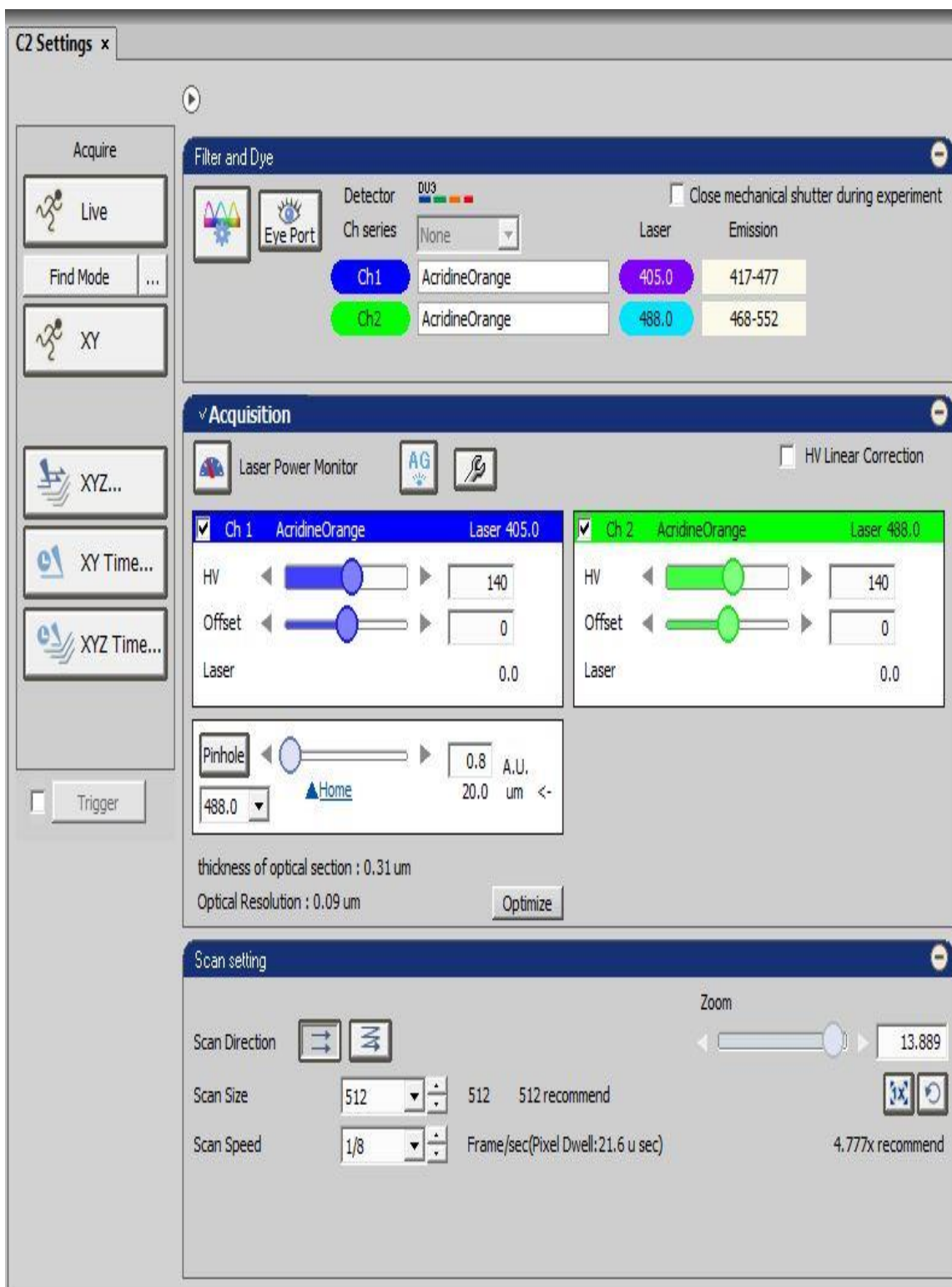
Figure 4.1 The image of the various parameters.

4.2 (a)) demonstrates much less details than the STED image which clearly discerns more singe nanoparticles.

We analyzed the resolution of the confocal an STED images. The resolution was measured by analyzing the profile intensity. The fluorescent profile intensities of nanoparticles were measured by line profiles along the traces which were indicated by the yellow arrows. The corresponding intensity profile is displayed in the Figure 4.3 (b) and (d).There have two methods to measure the resolution, one is the resolution is determined by the full-width-at-half-maximum, used in calculating the confocal resolution. The other one is that the resolution is determined by the samllest distance between two peaks can be discriminated, used in calculating the STED resolution. The Figure 4.2 (b) demonstrates that full-width-at-half-maximum value is about 206.21 nm. Whereas, the Figure 4.2(d) displays that the STED resolution could reach 76.51 nm. In comparison, the STED resolution has a great improvement. However, the STED resolution still is not enough ideal in our STED system. Because there still has a lot of disadvantages of STED system can be improved in the future.
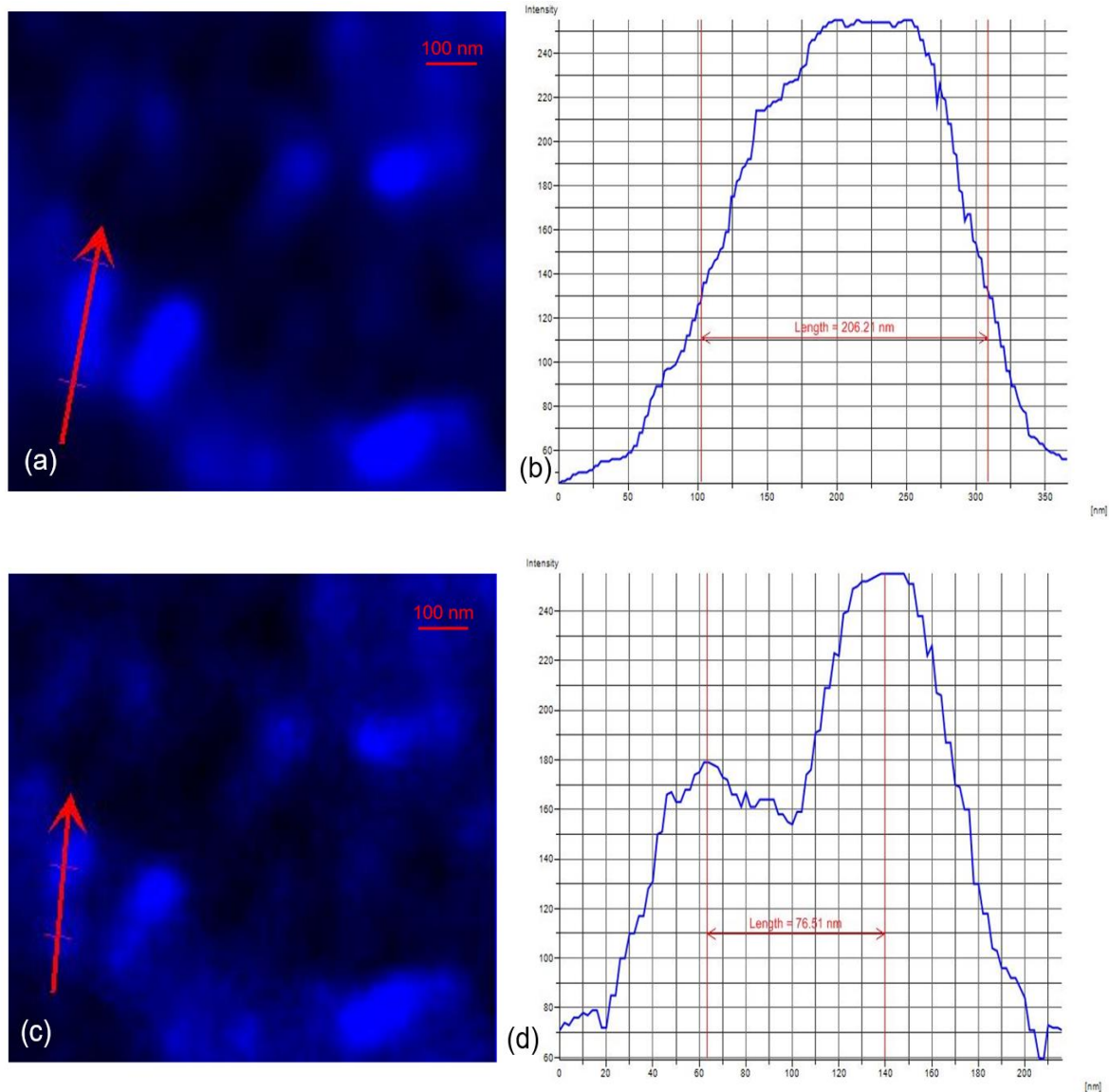
Figure 4.2 (a) the confocal image of LYs (b) the intensity profile along the yellow arrow in the confocal image (c) the STED image of LYs (d) the in tensity profile along the yellow arrow in the STED image.

4.2 DISCUSSION AND OUTLOOK

Based on the result, even though the STED resolution can reach 76.02 nm, we still notice that the signal-to-noise ratio is high in the Figure 4.2, leading to the low contrast. The other factors like the PMT, scan size, scan speed even the zoom have an important effect on the improvement of resolution of STED system. There is no doubt that the pinhole size plays a critical role in adjusting the signal intensity and the contrast of images. The STED resolution strongly depends on the size of the pinhole.

The reasons for using a pinhole are mainly to reject the out-of-focus light rays, for example, the stray and ambient light. As shown in the Figure 4.4, the resolution in X-Y plane is determined by the distance from the center of the Airy disk to the first dark ring. As a common knowledge, the pattern of Airy disk is relative to the first-order Bessel function of the first kind. The point spread function (PSF) is extracted along a horizontal line across the center of the Airy Disk, displaying in the Figure 4.4 (c).

Therefore, the width of the PSF---r is usually defined as the radial distance, for which the value of the paraxial PSF becomes zero (Ohtsu and Hori 1999), given by

$$r = 0.6098 \frac{m\lambda}{NA} \qquad (2)$$

where λ is the wavelength of the illumination light passing through the lens, and NA is the numerical aperture of the objective lens, m is the magnification of lens.
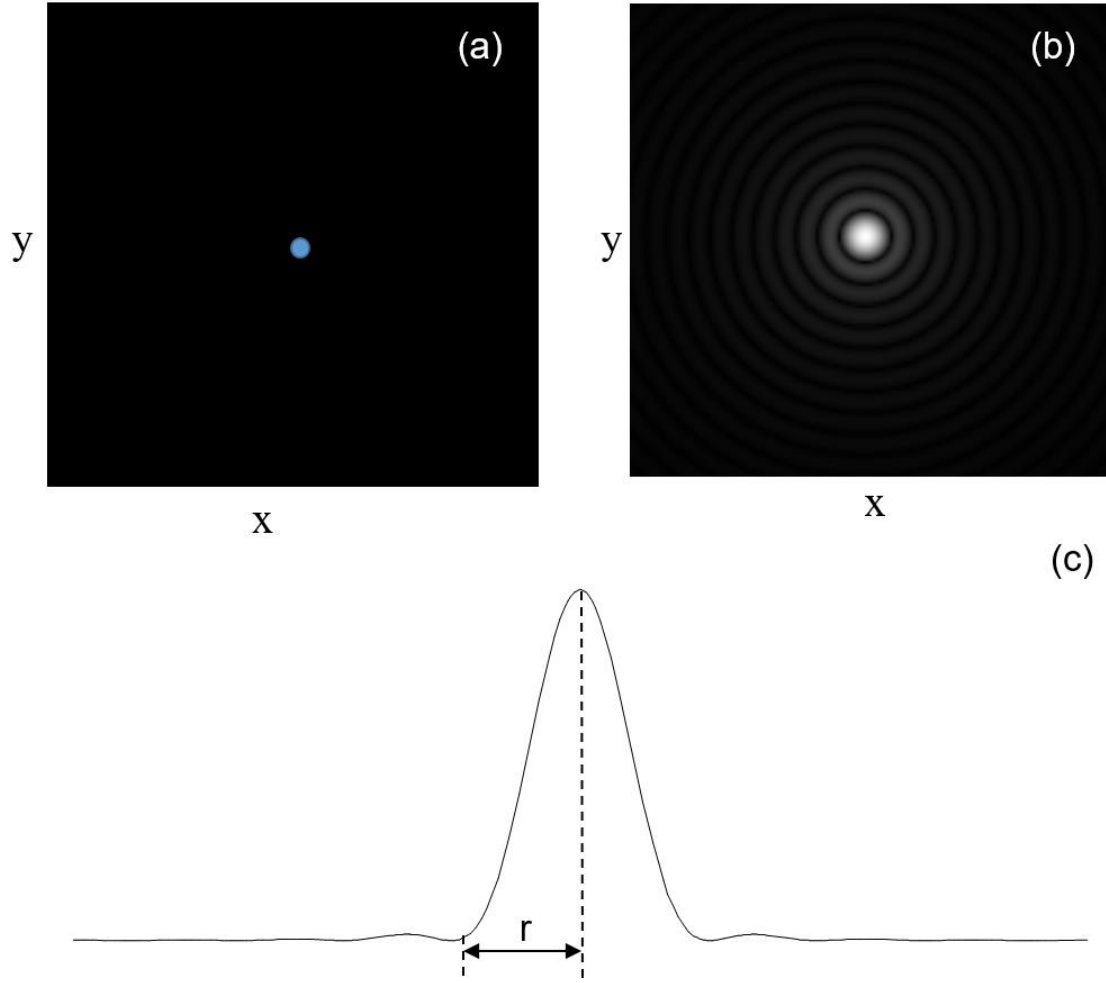
Figure 4.3 (a) the point source; (b) the diffraction pattern of the point source induced by the pinhole in the confocal plane; (c) the light intensity along a horizontal line across the center of the Airy Disk (Ohtsu and Hori 1999).

Therefore, the diameter of central disk is called one Airy unit (1AU), The 1AU can be theoretically described with the following equation:

$$1AU = 2r = 1.22\frac{m\lambda}{NA} \tag{3}$$

The Airy unit is defined in the Equation (2) and used primarily for normalizing the actual pinhole size in accordance with the light wavelength and the NA of the objective. At the beginning, we hypothesize that the pinhole size should be as small as

possible for improving the STED resolution. Yet, when the pinhole size decreased, the number of photons gettingto the detector from the specimen also reduced. Hence, this may lead to a decreased signal-to-noise ratio and the signal from the specimen also will reduce. For offsetting the weaker fluorescent intensity, much stronger fluorescence is needed from the specimen. The method usually can be employed by enhancing and elevating the power of the excitation light. High power of the excitation light can cause the degradation of fluorophores and the damage of the specimen. Therefore, a sufficiently small pinhole size is not always the best choice for the STED system.

Choosing suitable pinhole size is extremely important for STED system. The pinhole size cannot be too small for ensuring enough photons to be collected. The pinhole size cannot be too big, because the loss in contrast due to unwanted fluorescence from the neighboring regions.

For our STED system, the resolution is not enough high, the pinhole size is one of major reasons. In our STED system, the NA=1.4, the excitation wavelength is 405nm, the magnification of lens is 100. According to the equation (3), we calculated that the pinhole size (1AU) should be 35.3 um. In our experiment, the pinhole size we used is 20 um, approaching to 0.5 AU. Generally, the pinhole size of 1AU should be able to produce the best signal/noise. The pinhole size of 0.5AU has the possibility to improve the resolution if the signal is strong enough. However, our resolution is not high enough, the one reason is that the alignment is not good enough and has the space to be improved, producing high background noise and unwanted fluorescence from the neighboring part. Another reason is that as the pinhole size becomes small, the number of photons that arrive at the detector from the specimen also reduced. This can result in a reduced signal-to-noise ratio

(Pankajakshan 2010). The images obtained from the smaller pinhole (0.5AU), have an increase in contrast. Total signal collected is less as well (signal from the region of interest and out-of-focus signal). Thus, There has a trade-off to be established between the pinhole size, amount of noise and the out-of-focus light. Need to do more experiments for finding the most suitable pinhole size

When we use the smaller size of pinhole, the fluorescent signal is so weak that we almost cannot observe the pattern of specimen.   To offset the weaker signal, more fluorescence is needed from the specimen. This usually can be done, to a limit, by raising the intensity of the excitation light. However, high intensities can damage the specimen. In the case of fluorescence, high intensities also degrade the fluorophore. Meanwhile, when the pinhole size is a little big and the fluorescent intensity is strong, but the contrast will be lost.

One can notice that other factors like PMT HV, scanning speed and scanning size etc. These factors have an important effect on the resolution of STED system. Therefore, for the further work, we need to scan particle image and make further efforts to improve the image resolution with optimizing various parameters.

1. For the pinhole size, we used the 20 μm pinhole size in the previous experiment, we can compare with the resolution of STED images for three different sizes (20 μm, 30 μm and 40 μm) under the same situation, and then find out the most suitable pinhole size.

2. Then keep other factors fixed, just change the value of PMT HV to see the resolution change of STED images. Find out the most suitable value of PMT HV.

3. And then keep other factors fixed, find out the most suitable value of the scanning size, scanning speed and even the zoom for STED system.

4. Finally, use the most suitable value of all kinds of parameters to see if we can obtain the best resolution of STED system.

5. The Nikon-Element software has various functions, learn and use software to process and further improve image quality.

6. Excitation laser power is too small. We cannot detect the value by using the PowerMax-USB/RS sensors. We just use the polarizer number to indicate the power of excitation laser. Hope we could find a new method to measure the power of excitation laser.

7. We find that the gold nanoparticle specimen has the accumulation phenomenon. We will try to use some methods like adding the buffer solution to the specimen to reduce the aggregation.

8. One can notice that the background noise is a little high, hope we could discover some new methods to decrease the background noise and improve the signal-noise-rate.

9. The work could expand the application of STED. We will scan the cells and observe the detailed structure of the cells in the future.

10. Except the bio-imaging, CW-STED nanoscopy has also been successfully applied to nanoscopic measurement in micro- and nano-fluidics in our lab. For instance, laser induced fluorescence photo-bleaching anemometer (LIFPA) is a new method that can measure flow velocity with simultaneously high spatial and temporal resolution. With CW-STED microscopy, LIFPA has the potential

to measure the flow velocity profile in a nano-channel and interfacial flows, such as electrical double layers and slip flows. The pulsed STED microscopy should have the same application in the LIFPA. Therefore, we will detect the flow velocity with simultaneously high spatial and temporal resolution in the future.

11. Success in super-resolution imaging depends on the appropriate selection of fluorophores. A broad range of available fluorophores have been developed so far, but not all of them are applicable to STED microscopy. For example, not all dyes can be depleted with a second laser beam. Additionally, fluorophores should have high photo-stability. Therefore, it is highly desired that novel fluorophores can be developed which meet critical requirements for STED applications.

REFERENCE

Abbe, E. (1873). "Beiträge zur Theorie des Mikroskops und der mikroskopischen Wahrnehmung." Archiv für mikroskopische Anatomie 9(1): 413-418.

Agard, D. A. (1984). "Optical sectioning microscopy: cellular architecture in three dimensions." Annual review of biophysics and bioengineering 13(1): 191-219.

Agard, D. A. and J. W. Sedat (1983). "Three-dimensional architecture of a polytene nucleus." Nature 302(5910): 676-681.

Auksorius, E., B. R. Boruah, C. Dunsby, P. M. Lanigan, G. Kennedy, M. A. Neil and P. M. French (2008). "Stimulated emission depletion microscopy with a super-continuum source and fluorescence lifetime imaging." Optics letters 33(2): 113-115.

Betzig, E., G. H. Patterson, R. Sougrat, O. W. Lindwasser, S. Olenych, J. S. Bonifacino, M. W. Davidson, J. Lippincott-Schwartz and H. F. Hess (2006). "Imaging intracellular fluorescent proteins at nanometer resolution." Science 313(5793): 1642-1645.

Binnig, G. and H. Rohrer (1984). "Scanning tunneling microscopy." Physica B+ C 127 (1-3): 37-45.

Binnig, G. and H. Rohrer (1987). "Scanning tunneling microscopy—from birth to adolescence." reviews of modern physics 59(3): 615.

Brakenhoff, G., P. Blom and P. Barends (1979). "Confocal scanning light microscopy with high aperture immersion lenses." Journal of Microscopy 117(2): 219-232.

Brazelton, T. R. and H. M. Blau (2005). "Optimizing techniques for tracking transplanted stem cells in vivo." Stem cells 23(9): 1251-1265.

Bretschneider, S., C. Eggeling and S. W. Hell (2007). "Breaking the diffraction barrier in fluorescence microscopy by optical shelving." Physical review letters 98(21): 218103.

Busko, D., S. Baluschev, D. Crespy, A. Turshatov and K. Landfester (2012). "New possibilities for materials science with STED microscopy." Micron 43(5): 583-588.

Chen, X., M. Velliste, S. Weinstein, J. W. Jarvik and R. F. Murphy (2003). Location proteomics: building subcellular location trees from high-resolution 3D fluorescence

microscope images of randomly tagged proteins. Biomedical Optics 2003, International Society for Optics and Photonics

Cremer, C. and T. Cremer (1974). "Considerations on a laser-scanning-microscope with high resolution and depth of field." Microscopica acta: 31-44.

Dean, K. M. and A. E. Palmer (2014). "Advances in fluorescence labeling strategies for dynamic cellular imaging." Nature chemical biology 10(7): 512-523.

Denk, W., J. H. Strickler and W. W. Webb (1990). "Two-photon laser scanning fluorescence microscopy." Science 248(4951): 73-76.

Donnert, G., J. Keller, R. Medda, M. A. Andrei, S. O. Rizzoli, R. Lührmann, R. Jahn, C. Eggeling and S. W. Hell (2006). "Macromolecular-scale resolution in biological fluorescence microscopy." Proceedings of the National Academy of Sciences 103(31): 11440-11445.

Dudovich, N., D. Oron and Y. Silberberg (2002). "Single-pulse coherently controlled nonlinear Raman spectroscopy and microscopy." Nature 418(6897): 512-514.

Dyba, M. and S. W. Hell (2002). "Focal spots of size $\lambda/23$ open up far-field florescence microscopy at 33 nm axial resolution." Physical review letters 88(16): 163901.

Dyba, M., S. Jakobs and S. W. Hell (2003). "Immunofluorescence stimulated emission depletion microscopy." Nature biotechnology 21(11): 1303-1304.

Dyba, M., J. Keller and S. Hell (2005). "Phase filter enhanced STED-4Pi fluorescence microscopy: theory and experiment." New Journal of Physics 7(1): 134.

Freeman, R., T. Finder, R. Gill and I. Willner (2010). "Probing protein kinase (CK2) and alkaline phosphatase with CdSe/ZnS quantum dots." Nano letters 10(6): 2192-2196.

Gustafsson, M. G. (2005). "Nonlinear structured-illumination microscopy: wide-field fluorescence imaging with theoretically unlimited resolution." Proceedings of the National Academy of Sciences of the United States of America 102(37): 13081-13086.

Gustafsson, M. G., L. Shao, P. M. Carlton, C. R. Wang, I. N. Golubovskaya, W. Z. Cande, D. A. Agard and J. W. Sedat (2008). "Three-dimensional resolution doubling in wide-field fluorescence microscopy by structured illumination." Biophysical journal 94(12): 4957-4970.

Harke, B. (2008). "3D STED microscopy with pulsed and continuous wave lasers." Georg-August-University Goettingen, Goettingen.

Harke, B., J. Keller, C. K. Ullal, V. Westphal, A. Schönle and S. W. Hell (2008). "Resolution scaling in STED microscopy." Optics express 16(6): 4154-4162.

Hell, S. and E. H. Stelzer (1992). "Fundamental improvement of resolution with a 4Pi-confocal fluorescence microscope using two-photon excitation." Optics Communications 93(5-6): 277-282.

Hell, S. and E. H. Stelzer (1992). "Properties of a 4Pi confocal fluorescence microscope." JOSA A 9(12): 2159-2166.

Hell, S. W. (2007). "Far-field optical nanoscopy." science 316(5828): 1153-1158.

Hell, S. W. (2009). "Microscopy and its focal switch." Nature methods 6(1): 24-32.

Hell, S. W., M. Booth, S. Wilms, C. M. Schnetter, A. K. Kirsch, D. J. Arndt-Jovin and T. M. Jovin (1998). "Two-photon near-and far-field fluorescence microscopy with continuous-wave excitation." Optics letters 23(15): 1238-1240.

Hell, S. W., M. Dyba and S. Jakobs (2004). "Concepts for nanoscale resolution in fluorescence microscopy." Current opinion in neurobiology 14(5): 599-609.

Hell, S. W. and M. Kroug (1995). "Ground-state-depletion fluorscence microscopy: A concept for breaking the diffraction resolution limit." Applied Physics B: Lasers and Optics 60(5): 495-497.

Hell, S. W. and E. Rittweger (2009). "Microscopy: Light from the dark." Nature 461(7267): 1069-1070.

Hell, S. W. and J. Wichmann (1994). "Breaking the diffraction resolution limit by stimulated emission: stimulated-emission-depletion fluorescence microscopy." Optics letters 19(11): 780-782.

Hopt, A. and E. Neher (2001). "Highly nonlinear photodamage in two-photon fluorescence microscopy." Biophysical journal 80(4): 2029-2036.

Hotta, J.-i., E. Fron, P. Dedecker, K. P. Janssen, C. Li, K. Müllen, B. Harke, J. Bückers, S. W. Hell and J. Hofkens (2010). "Spectroscopic rationale for efficient stimulated-emission depletion microscopy fluorophores." Journal of the American Chemical Society 132(14): 5021-5023.

Huang, F. M. and N. I. Zheludev (2009). "Super-resolution without evanescent waves." Nano letters 9(3): 1249-1254.

Irvine, S. E., T. Staudt, E. Rittweger, J. Engelhardt and S. W. Hell (2008). "Direct light‑driven modulation of luminescence from Mn‑doped ZnSe quantum dots." Angewandte Chemie 120(14): 2725-2728.

Kellner, R., C. Baier, K. Willig, S. Hell and F. Barrantes (2007). "Nanoscale organization of nicotinic acetylcholine receptors revealed by stimulated emission depletion microscopy." Neuroscience 144(1): 135-143.

Kimura, S. and C. Munakata (1989). "Calculation of three-dimensional optical transfer function for a confocal scanning fluorescent microscope." JOSA A 6(7): 1015-1019.

Kinosita, K., I. Ashikawa, N. Saita, H. Yoshimura, H. Itoh, K. Nagayama and A. Ikegami (1988). "Electroporation of cell membrane visualized under a pulsed-laser fluorescence microscope." Biophysical journal 53(6): 1015-1019.

Kircher, M. F., U. Mahmood, R. S. King, R. Weissleder and L. Josephson (2003). "A multimodal nanoparticle for preoperative magnetic resonance imaging and intraoperative optical brain tumor delineation." Cancer research 63(23): 8122-8125.

Klar, T. A., E. Engel and S. W. Hell (2001). "Breaking Abbe's diffraction resolution limit in fluorescence microscopy with stimulated emission depletion beams of various shapes." Physical Review E 64(6): 066613.

Klar, T. A. and S. W. Hell (1999). "Subdiffraction resolution in far-field fluorescence microscopy." Optics letters 24(14): 954-956.

Klar, T. A., S. Jakobs, M. Dyba, A. Egner and S. W. Hell (2000). "Fluorescence microscopy with diffraction resolution barrier broken by stimulated emission." Proceedings of the National Academy of Sciences 97(15): 8206-8210.

Kobayashi, H., M. Ogawa, R. Alford, P. L. Choyke and Y. Urano (2009). "New strategies for fluorescent probe design in medical diagnostic imaging." Chemical reviews 110(5): 2620-2640.

Kuang, C., W. Zhao and G. Wang (2010). "Far-field optical nanoscopy based on continuous wave laser stimulated emission depletion." Review of Scientific Instruments 81(5): 053709.

Lewis, A., M. Isaacson, A. Harootunian and A. Muray (1984). "Development of a 500 Å spatial resolution light microscope: I. light is efficiently transmitted through λ/16 diameter apertures." Ultramicroscopy 13(3): 227-231.

Li, W., R. Liu, Y. Wang, Y. Zhao and X. Gao (2013). "Temporal techniques: dynamic tracking of nanomaterials in live cells." Small 9(9‐10): 1585-1594.

Lichtman, J. W. and J.-A. Conchello (2005). "Fluorescence microscopy." Nature methods 2(12): 910-919.

Meyer, L., D. Wildanger, R. Medda, A. Punge, S. O. Rizzoli, G. Donnert and S. W. Hell (2008). "Dual‐Color STED Microscopy at 30‐nm Focal‐Plane Resolution." Small 4(8): 1095-1100.

Moneron, G., R. Medda, B. Hein, A. Giske, V. Westphal and S. W. Hell (2010). "Fast STED microscopy with continuous wave fiber lasers." Optics express 18(2): 1302-1309.

Nagano, T. (2009). "Bioimaging probes for reactive oxygen species and reactive nitrogen species." Journal of clinical biochemistry and nutrition 45(2): 111-124.

Novotny, L., E. J. Sánchez and X. S. Xie (1998). "Near-field optical imaging using metal tips illuminated by higher-order Hermite–Gaussian beams." Ultramicroscopy 71(1): 21-29.

Ohtsu, M. and H. Hori (1999). Principles of Near-Field Optical Microscopy. Near-Field Nano-Optics, Springer: 43-61.

Pankajakshan, P. (2010). Blind deconvolution for confocal laser scanning microscopy, Citeseer.

Pohl, D. W. and D. Courjon (2012). Near field optics, Springer Science & Business Media.

Pohl, D. W., W. Denk and M. Lanz (1984). "Optical stethoscopy: Image recording with resolution λ/20." Applied physics letters 44(7): 651-653.

Punge, A., S. O. Rizzoli, R. Jahn, J. D. Wildanger, L. Meyer, A. Schönle, L. Kastrup and S. W. Hell (2008). "3D reconstruction of high‐resolution STED microscope images." Microscopy research and technique 71(9): 644-650.

Rankin, B. R., R. R. Kellner and S. W. Hell (2008). "Stimulated-emission-depletion microscopy with a multicolor stimulated-Raman-scattering light source." Opt Lett 33(21): 2491-2493.

Rankin, B. R., R. R. Kellner and S. W. Hell (2008). "Stimulated-emission-depletion microscopy with a multicolor stimulated-Raman-scattering light source." Optics letters 33(21): 2491-2493.

Rankin, B. R., G. Moneron, C. A. Wurm, J. C. Nelson, A. Walter, D. Schwarzer, J. Schroeder, D. A. Colón-Ramos and S. W. Hell (2011). "Nanoscopy in a living multicellular organism expressing GFP." Biophysical journal 100(12): L63-L65.

Rittweger, E., K. Y. Han, S. E. Irvine, C. Eggeling and S. W. Hell (2009). "STED microscopy reveals crystal colour centres with nanometric resolution." Nature Photonics 3(3): 144-147.

Salerno, D. and J.-R. Daban (2003). "Comparative study of different fluorescent dyes for the detection of proteins on membranes using the peroxyoxalate chemiluminescent reaction." Journal of Chromatography B 793(1): 75-81.

Santra, S., D. Dutta, G. A. Walter and B. M. Moudgil (2005). "Fluorescent nanoparticle probes for cancer imaging." Technology in cancer research & treatment 4(6): 593-602.

Sheppard, C. and R. Kompfner (1978). "Resonant scanning optical microscope." Applied optics 17(18): 2879-2882.

Shtengel, G., J. A. Galbraith, C. G. Galbraith, J. Lippincott-Schwartz, J. M. Gillette, S. Manley, R. Sougrat, C. M. Waterman, P. Kanchanawong and M. W. Davidson (2009). "Interferometric fluorescent super-resolution microscopy resolves 3D cellular ultrastructure." Proceedings of the National Academy of Sciences 106(9): 3125-3130.

Stokes, G. (1853). "On the change of refrangibility of light. No. II." Philosophical Transactions of the Royal Society of London 143: 385-396.

Takasaki, K. T., J. B. Ding and B. L. Sabatini (2013). "Live-cell superresolution imaging by pulsed STED two-photon excitation microscopy." Biophys J 104(4): 770-777.

Tzeng, Y. K., O. Faklaris, B. M. Chang, Y. Kuo, J. H. Hsu and H. C. Chang (2011). "Superresolution Imaging of Albumin‐Conjugated Fluorescent Nanodiamonds in Cells by Stimulated Emission Depletion." Angewandte Chemie International Edition 50(10): 2262-2265.

Vaijayanthimala, V. and H. Chang (2009). "Functionalized fluorescent nanodiamonds for biomedical applications." Nanomedicine 4(1): 47-55.

Velliste, M. and R. F. Murphy (2002). Automated determination of protein subcellular locations from 3D fluorescence microscope images. Biomedical Imaging, 2002. Proceedings. 2002 IEEE International Symposium on, IEEE.

Vicidomini, G., G. Moneron, K. Y. Han, V. Westphal, H. Ta, M. Reuss, J. Engelhardt, C. Eggeling and S. W. Hell (2011). "Sharper low-power STED nanoscopy by time gating." Nature methods 8(7): 571-573.

WA, R. (1959). "Principles of optics."

Watanabe, S., A. Punge, G. Hollopeter, K. I. Willig, R. J. Hobson, M. W. Davis, S. W. Hell and E. M. Jorgensen (2011). "Protein localization in electron micrographs using fluorescence nanoscopy." Nature methods 8(1): 80-84.

Westphal, V., C. Blanca, M. Dyba, L. Kastrup and S. Hell (2003). "Laser-diode-stimulated emission depletion microscopy." Applied Physics Letters 82(18): 3125-3127.

Westphal, V. and S. W. Hell (2005). "Nanoscale resolution in the focal plane of an optical microscope." Phys Rev Lett 94(14): 143903.

Westphal, V. and S. W. Hell (2005). "Nanoscale resolution in the focal plane of an optical microscope." Physical review letters 94(14): 143903.

Westphal, V., L. Kastrup and S. W. Hell (2003). "Lateral resolution of 28 nm (?/25) in far-field fluorescence microscopy." Applied Physics B: Lasers and Optics 77(4): 377-380.

Westphal, V., S. O. Rizzoli, M. A. Lauterbach, D. Kamin, R. Jahn and S. W. Hell (2008). "Video-rate far-field optical nanoscopy dissects synaptic vesicle movement." Science 320(5873): 246-249.

Westphal, V., J. Seeger, T. Salditt and S. W. Hell (2005). "Stimulated emission depletion microscopy on lithographic nanostructures." Journal of Physics B: Atomic, Molecular and Optical Physics 38(9): S695.

Wildanger, D., J. Bückers, V. Westphal, S. W. Hell and L. Kastrup (2009). "A STED microscope aligned by design." Optics Express 17(18): 16100-16110.

Wildanger, D., R. Medda, L. Kastrup and S. Hell (2009). "A compact STED microscope providing 3D nanoscale resolution." Journal of microscopy 236(1): 35-43.

Wildanger, D., E. Rittweger, L. Kastrup and S. W. Hell (2008). "STED microscopy with a supercontinuum laser source." Opt Express 16(13): 9614-9621.

Wildanger, D., E. Rittweger, L. Kastrup and S. W. Hell (2008). "STED microscopy with a supercontinuum laser source." Optics express 16(13): 9614-9621.

Williams, R. M., W. R. Zipfel and W. W. Webb (2001). "Multiphoton microscopy in biological research." Current opinion in chemical biology 5(5): 603-608.

Willig, K. I., B. Harke, R. Medda and S. W. Hell (2007). "STED microscopy with continuous wave beams." Nat Methods 4(11): 915-918.

Willig, K. I., B. Harke, R. Medda and S. W. Hell (2007). "STED microscopy with continuous wave beams." Nature methods 4(11): 915-918.

Willig, K. I., S. O. Rizzoli, V. Westphal, R. Jahn and S. W. Hell (2006). "STED microscopy reveals that synaptotagmin remains clustered after synaptic vesicle exocytosis." Nature 440(7086): 935-939.

Wilson, T. and C. Sheppard (1984). Theory and practice of scanning optical microscopy, Academic Press London.

Wolfbeis, O. S. (2015). "An overview of nanoparticles commonly used in fluorescent bioimaging." Chemical Society Reviews 44(14): 4743-4768.

Wright, S. J., V. E. Centonze, S. A. Stricker, P. J. DeVries, S. W. Paddock and G. Schatten (1993). "Introduction to confocal microscopy and three-dimensional reconstruction." Methods in cell biology 38: 1-45.

Xie, H., Y. Liu, D. Jin, P. J. Santangelo and P. Xi (2013). "Analytical description of high-aperture STED resolution with 0–2π vortex phase modulation." JOSA A 30(8): 1640-1645.

Xing, Y. and L. Dai (2009). "Nanodiamonds for nanomedicine."

Xu, J., J. Wang, M. Mitchell, P. Mukherjee, M. Jeffries-EL, J. W. Petrich and Z. Lin (2007). "Organic− inorganic nanocomposites via directly grafting conjugated polymers onto quantum dots." Journal of the American Chemical Society 129(42): 12828-12833.